Organometallic gold(III) [Au(Hdamp)(L1^4)]Cl (L1 = *SNS*-donating thiosemicarbazone) complex protects mice against acute *T. cruzi* infection

Carla Duque Lopes[a,e], Ana Paula S. Gaspari[a,f], Ronaldo J. Oliveira[b], Ulrich Abram[c], José P. A. Almeida[d], Pedro v. S. Maia[b], João S. da Silva[e], Sérgio de Albuquerque[a], Zumira A. Carneiro[a,d*‡]

Department of Clinical Toxicological and Bromatological Analysis School of Pharmaceutical Sciences of Ribeirão Preto, University of São Paulo (USP), Ribeirão Preto, Brazil[a]; Núcleo de Desenvolvimento de Compostos Bioativos (NDCBio), Universidade Federal do Triângulo Mineiro, Uberaba – MG, Brazil[b]; Freie Universität Berlin, Institute of Chemistry and Biochemistry, Berlin, Germany[c]; Centro Universitário Estácio de Ribeirão Preto, SP, Brazil[d]; Departament of Biochemistry and Immunology, School of Medicine, University of São Paulo, Ribeirão Preto, São Paulo, Brazil[e]; Departamento de Química, Faculdade de Filosofia, Ciências e Letras de Ribeirão Preto – FFCLRP-USP, University of São Paulo, Ribeirão Preto, SP, Brazil[f].

Running Title: Gold complex protects from *T. cruzi* infection

‡ These authors contributed equally

*Address correspondence to Zumira Carneira, carneirozumira@gmail.com

Abstract

Chagas disease remains a serious public health concern with unsatisfactory treatment outcomes due to strain-specific drug resistance and various side effects. To identify new therapeutic drugs against *Trypanosoma cruzi*, we evaluated both the *in vitro* and *in vivo* activity of the organometallic gold(III) complex [Au(Hdamp)($L1^4$)]Cl (L1 = *SNS*-donating thiosemicarbazone), which was denoted 4-Cl. Our results demonstrated that 4-Cl was more effective than benznidazole (Bz) in eliminating both the extracellular trypomastigote and the intracellular amastigote forms of the parasite without cytotoxic effects on mammalian cells. In very-low-dose *in vivo* assays, 4-Cl reduced parasitaemia and tissue parasitism in addition to protecting the liver and heart from tissue damage. All these changes resulted in the survival of 100% of the mice treated with 4-Cl during the acute phase. We hypothesised that 4-Cl can act directly on the parasite and may participate in the modulation of IFN-γ production at the acute stage of the disease. Molecular docking simulations showed that the compound may interact with cruzain, a thiol protease considered a possible antiparasitic drug target, primarily by hydrophobic interactions. These analyses predicted that the Cys25 residue in the cruzain binding site is approximately 3.0 Å away from the S and Au atoms of the gold compound, which could suggest formation of a possible covalent bond between cruzain and the inhibitor. Overall, we confirmed the potential of 4-Cl as a new candidate for Chagas disease treatment.

Keywords: Gold(III) Complex, Thiosemicarbazones, Chagas disease, Trypanocidal activity, immune response, IFN-γ production.

Introduction

Chagas disease is a neglected infection caused by a protozoan parasite named *Trypanosoma cruzi (T. cruzi)*, transmitted by triatomine insect vectors, which is endemic in Latin America. According to the World Health Organization (WHO), approximately ten million people are infected with *T. cruzi* worldwide(1, 2). In addition, the phenomena of globalization and immigration have also led to the appearance of several infectious cases in development of the disease(2). Currently, only two drugs are available for the treatment of the Chagas disease: nifurtimox (NFX) and benznidazole (Bz)(3, 4). In some countries, NFX was discontinued due to serious side effects, such as neuropathy and anorexia, among others(5, 6). Thus, the only drug currently used for therapeutic purposes is Bz which is effective only during the acute phase of the infection but may present undesirable systemic toxicity, such as rashes and gastrointestinal symptoms(6). Therefore, the development of more efficacious and less toxic drugs, which can be used as alternatives for drug resistance, is urgently needed(7, 8).

A potential strategy for the treatment of Chagas disease is the design of compounds that selectively inhibit essential enzymes for parasite survival inside the host cells(9). In the case of *T. cruzi*, cruzain is an attractive drug target. The structure of cruzain contains a cysteine protease domain, which plays an important role during the life cycle of the parasite, such as replication, metabolism, and evasion of host immune defence during the early events of macrophage infection(10). Although many other potential drug targets exist in parasite metabolism(8), cruzain is by far the most studied protease of *T. cruzi* due to its role as a virulence factor of the parasite(9). Thus, compounds that inhibit the biological function of cruzain, such as thiosemicarbazones, may be an effective

alternative for pharmacological treatment of Chagas disease(6, 7). In this context, transition metal complexes that have thiosemicarbazones as ligands have been developed and tested against various forms of *T. cruzi* (8, 9). Gold(III) complexes have received increased attention due to their biological properties, such as anti-cancer(11) and antiparasitic effects(12). In a recent paper, our research group identified complexes of the general formula [Au^{III}(Hdamp)(L1)]Cl (Fig. 1) that have high stability in aqueous solution and antiparasitic activity against the *Tulahuen LacZ* strain. Among these compounds, 4-Cl, [Au^{III}(Hdamp)($R_1R_2L1^4$)]Cl (R_1 = R_2 = Methyl) demonstrated low cytotoxicity in spleen cells, leading to a selectivity index (SI) of approximately 30(8), which indicated that this compound is a promising candidate for the development of trypanocidal drugs.

Fig. 1. Organometallic gold(III) complexes containing hybrid *SNS*-donating thiosemicarbazone ligands [Au^{III}(Hdamp)(L1)]Cl (Hdamp = dimethylammoniummethylphenyl) (Adapted from (8)).

Clinical manifestations associated with *T. cruzi* infection are dependent on the intricate equilibrium between the parasite and the host immune response. The production of interferon gamma (IFN-γ) generated for adaptive immune responses is important for inhibition of parasite proliferation(13, 14). Intense production of IFN-γ activates the CD4 T lymphocytes with s Type 1 Helper T (Th1) profile and cytotoxic CD8 T lymphocytes, which efficiently eliminate the parasite (15). T-Helper 17 (Th17) cells have the potential to become antigen-specific CD8 T cells against the parasite and show greater contributions than the subpopulation of CD4 T cells, which are producers of IFN-γ. Consequently, their cytotoxic and cytokine secretion functions are decreased,

hindering parasite elimination (16). Therefore, the modulation of immune responses is fundamental for a good prognosis of Chagas disease.

Since the acute phase of Chagas disease has been associated with *T. cruzi* II-restricted infections, in the present study, the *in vitro* and *in vivo* 4-Cl trypanocidal activity was evaluated against the Y strain (group TcII) to assess the use of this compound as a new drug for the treatment of Chagas disease. Docking studies were also conducted to elucidate the interaction between the gold(III) complex with the *T. cruzi* enzyme cruzain (18). Based on the cruzain inhibitory potential of thiosemicarbazone-derived compounds, molecular docking techniques were employed on this enzyme to identify the possible target of [Au(Hdamp)($L1^4$)]Cl in the parasite.

Results

The gold complex acts directly on *T. cruzi* parasites

The organometallic gold(III) complex 4-Cl has interesting characteristics from both chemical and biological points of view (8). Then, we initially assessed the effectiveness of 4-Cl against the *T. cruzi* Y strain, which is partially resistant to Bz treatment and more virulent than the *Tulahuen* strain. The trypomastigotes of the Y strain were incubated with serial dilutions of 4-Cl or Bz for 24 h, and live parasites were counted by colorimetric analyses. The 4-Cl treatment was highly efficient compared to Bz treatment, reaching an IC_{50Try} (concentration needed to kill 50% of the parasites) of 0.03±0.006 µM, whereas the IC_{50Try} of Bz was 0.96±0.025 µM; these results indicate that 4-CL is almost thirty-two times more effective than Bz in killing the trypomastigote forms of *T. cruzi* (Fig. 2A). To determine the effects of 4-Cl on intracellular amastigotes of the *T. cruzi* Y strain, BMMs were differentiated and infected with the trypomastigote

124 forms for 16 h. The extracellular parasites were removed by extensive washes and
125 incubated with low concentrations of 4-Cl or Bz for 24 hours. The Bz treatment
126 maintained the same percentage of parasite killing at both concentrations, and its
127 trypanocidal capacity decreased with subsequent concentrations. At 3.2 µM, 4-Cl killed
128 75% of the intracellular amastigotes of *T. cruzi* and was more efficient than Bz (54%
129 inhibition of the replication or survival of the amastigotes). This high efficacy remained
130 until a concentration of 1.56 µM, and its trypanocidal activity was reduced only at
131 nanomolar concentrations (Fig. 2B). Interesting, the gold(III) complex at the highest
132 concentrations lost its ability to eliminate the intracellular parasites. This phenomenon
133 was not due to cytotoxicity in macrophages, whose the $EC_{50(4\text{-}Cl)}$ was 70 µM, relatively
134 close to the EC_{50} in primary culture of spleen cells (113 µM) (8). Most likely, at this
135 high concentration, there is a saturation of the absorption of the compound, which is no
136 longer effective in eliminating the parasite. The same phenomenon was observed for the
137 highest concentration of Bz (Fig. 2B). Therefore, by excluding the values of 6.2 µM to
138 obtain a real $IC_{50,}$ for both compounds, we obtained an $IC_{50(ama)}$ of 0.5 µM for 4-Cl,
139 indicating a trypanocidal activity 3.6 times higher than that of Bz ($IC_{50(ama)}$ of 1.8 µM).
140 Together, these data indicate that 4-Cl is more efficient in killing both mammalian
141 forms of the Y strain of *T. cruzi* than Bz.
142
143 **Fig. 2**. ***In vitro*** **trypanocidal activity of 4-Cl against the trypomastigote and**
144 **amastigote forms of the Y strain of *T. cruzi*.** (A) Percentage of trypanocidal activity
145 of 4-Cl and Bz against the Y strain of *T. cruzi* analysed by quantifying viable parasites
146 24 h post-treatment. (B) Macrophages derived from bone marrow were infected with the
147 trypomastigote form of the Y strain of *T. cruzi*. After 24 hours of infection, the

148 extracellular parasites were removed, and cells were infected with the amastigote forms
149 and treated with 4-Cl or Bz. Assays were conducted using biological replicates.
150
151 **The 4-Cl treatment protects the mice from *T. cruzi* infection**
152 The high efficiency of this treatment in eliminating both trypomastigote and amastigote
153 forms *in vitro* prompted us to investigate the potential of 4-Cl *in vivo*. For these
154 analyses, mice were infected with 2000 blood-derived trypomastigote forms of the Y
155 strain and orally treated with 2.8 mg/kg/day of 4-Cl, two different concentrations of Bz,
156 2.8 mg/kg/day of Bz(-) or 100 mg/kg/day of Bz(+) for 10 consecutive days from the
157 fifth day of infection (first point of parasitaemia). To optimise the treatment dose of 4-
158 Cl, we administered different concentrations to the mice based on the clinical dose of
159 Bz(+). At the highest doses, 4-Cl showed several toxicities and did not control the
160 parasitaemia (Fig S1). However, at a dose of 2.8 mg/kg, 4-Cl eliminated 61.3% of the
161 circulating parasites at the peak of infection (9 d.p.i.), while Bz(-) showed no reduction
162 compared to that of the PBS group (Fig. 3A). To determine whether the blood reduction
163 of parasites in 4-Cl-treated mice was reflected in the *T. cruzi* migration to skeletal
164 tissues, we performed a qPCR analysis specific to *T. cruzi* DNA in the heart and skeletal
165 muscle after 15 d.p.i. The number of copies found in the heart of 4-Cl-treated mice was
166 similar to Bz(-) treatment but was significantly less than that of the PBS-treated group
167 (Fig. 3B). In skeletal muscle, 4-Cl significantly reduced the parasitism compared with
168 both Bz(-) and PBS, showing that a low dose of 4-Cl is effective at preventing the
169 systemic spread of *T. cruzi* (Fig. 3C). Interestingly, evaluation of the heart histological
170 sections showed that the number of nests of both 4-Cl- and Bz(-)-treated mice was
171 reduced (Fig. 3D). Heart histological analysis revealed that amastigote nests (Fig. 3E-G)
172 decreased in all treated groups compared to the controls (Figure 3E). The amastigote

173 nests in the Bz(-) treatment group were the smallest and most scattered (Fig. 3F), in
174 contrast to the findings for the 4-Cl group, which showed the largest and most
175 individualised nests (Fig. 3G) which may justify that same amount of *T. cruzi* DNA was
176 found in the Bz(-) and 4-Cl heart samples (Fig. 3B).
177 Infection with the Y strain was shown to generate intense inflammatory infiltrates with
178 few amastigote nests, isolates or small groups (19) as observed in the PBS and Bz(-)
179 heart sections (Fig. 3E-F). In 4-Cl treatment, the presence of isolate nests was also
180 accompanied by a strong inflammatory infiltrate (Fig. 3G). When the survival of treated
181 mice was evaluated, we observed that 4-Cl protected the animals from the acute phase
182 of infection, while all mice succumbed to the infection after Bz(-) treatment as well as
183 the PBS treatment. This protection conferred by 4-Cl was the same as that of Bz at its
184 optimised dose (100 mg/kg/day), referred to as Bz(+) (Fig. 4A). After 150 days post-
185 infection, the hearts of the animals treated in the acute phase that survived the infection
186 were removed, and *T. cruzi* DNA was measured. The parasite load were detected, and
187 the levels in the hearts of 4-Cl-treated mice were as low as those in Bz(+)-treated mice
188 (Fig. 4B), although it was not possible to observe either the amastigote nests or the
189 inflammatory infiltrate in the heart of both treated groups (Fig S2). These differences
190 between high parasitaemia and low parasitism in the Bz(-) treatment can indicate that
191 the trypanocidal effects of Bz probably occur throughout the treatment, shortly after the
192 peak of infection, since the mice continued to be treated until they were sacrificed. In
193 the thirteenth d.p.i, the parasite levels in the blood of the Bz(-) group showed a
194 reduction compared to the PBS-treated mice, although this reduction was not
195 statistically significant (Fig. 3A).
196 In the chronic phase, the Bz(+)-treated mice tended to show an increased cardiac
197 parasitic burden compared to 4-Cl-treated mice (Fig. 4B). Another point to highlight is

198 the number of parasite nests found in the cardiac tissue of treated mice. In the
199 histopathological sections, Bz(-)-treated mice presented large numbers of nests with a
200 reduced area compared to 4-Cl-treated mice (Fig. 3F and 3G). These smaller nests with
201 greater quantities (Fig. 3D) may have resulted in a similar quantification of parasites in
202 the PCR assay between Bz(+)- and 4-Cl treated mice (Fig. 4B). Together, these data
203 suggest that the 4-Cl treatment in the acute phase protects the mice from lethal *T. cruzi*
204 infection.
205
206 **Fig. 3. Parasitic burden in the blood and tissue of infected mice after treatment**
207 **with 2.8 mg/kg/day of 4-Cl, 2.8 mg/kg/day of Bz(-) and 100 mg/kg/day of Bz(+)**
208 **during the acute phase of infection.** (A) Results indicated the decrease in parasitaemia
209 of animals treated with 4-Cl. Parasitaemia was monitored on days 7, 9, 11 and 13 after
210 infection. (B) Quantification of the parasite burden in cardiac tissues via real-time
211 qPCR. The presence of *T. cruzi* in infected heart tissues of mice was analysed by qPCR
212 15 d.p.i. (C) Quantification of the parasite burden in skeletal tissues via real-time qPCR.
213 The presence of *T. cruzi* in infected skeletal tissues of the mice was analysed by qPCR
214 15 d.p.i. (D) Number of amastigote nests in heart tissue. (E) Heart histological section
215 of PBS-treated mice, (F) Bz(-)-treated mice and (G), 4-Cl-treated mice. Arrows indicate
216 amastigote nests. The mean±SEM is shown and represents three independent
217 experiments (n=5). Significance was defined when *$p \leq 0.05$.
218
219 **Fig. 4. The 4-Cl treatment protects the mice from *T. cruzi* infection.** (A) *T. cruzi*-
220 infected mice (n=7) were treated for 10 consecutive days, from the fifth day after
221 infection, with a Bz(-) concentration of 2.8 mg/kg, a Bz(+) concentration of 100 mg/kg
222 (positive control), a 4-Cl concentration of 2.8 mg/kg and PBS. The mice were followed

223 up for 150 days to evaluate survival. (B) *T. cruzi* DNA quantification in the hearts of
224 surviving mice (n=3).
225
226 **4-Cl do not show tissue toxicity**
227 Analysis of toxicity is essential for the evaluation and development of new drugs for the
228 treatment of diseases. One way to evaluate the toxicity *in vivo* is to quantify the activity
229 of the enzyme Aspartate Aminotransferase (AST), which is detected in the cytoplasm
230 and mitochondria of a variety of tissues, such as the liver, heart, skeletal muscle,
231 pancreas, and red blood cells, and, therefore, is indicative of systemic damage (17)
232 There was no difference in toxicity between the treatments (Fig S3), revealing that the
233 high levels of AST found may be due to the *T. cruzi* systemic effects (20). However,
234 Alanine Aminotransferase (ALT) is primarily a liver-specific enzyme. The
235 organometallic treatment, similarly to Bz(-), reduced the ALT levels in the serum of
236 infected mice after 15 d.p.i. (Fig 5A). Interesting, this reduction continuous expressive
237 when compared to Bz(+) treated mice after 150 d.p.i (Fig 5B).
238 In the other hand, skeletal muscle is the target tissue in the *T. cruzi* infection. Serum
239 analysis of 4-Cl infected-treated mice showed a significant reduction of CK-MB, the
240 enzyme released into the plasma during cardiac lesion, in acute phase (Fig 5C) and
241 reduced 3 times the CK-MB levels in the surviving-treated mice (150 d.p.i) as compared
242 to Bz(+) treated mice (Fig 5D). Together, these data reinforce a protective role of 4-Cl
243 treatment.
244
245 **Fig. 5. Liver and cardiac lesions of *T. cruzi*-infected mice after treatment with 4-Cl.**
246 Quantification of (A) Alanine Aminotransferase (ALT) 15 d.p.i. (acute phase), (B)
247 Alanine Aminotransferase (ALT) 150 d.p.i. (chronic phase), (C) CK-MB (U/L) at 15

d.p.i. and (D) CK-MB (U/L) at 150 d.p.i. The data are represented as the mean ± SEM of three independent experiments, (n=5), using Student's t test and Mann-Whitney *post test* analysis. Data were considered significant when $p<0.05$. (*) indicates difference from PBS-treated mice and (&) differences from the Bz(+)-treated group.

High levels of IFNγ are detected in the early stage of acute infection after 4-Cl treatment

Studies suggest that the treatment in cooperation with host immune system has a large impact on the clearance of parasite (21, 22). Th17 cells act early in the infection by releasing IL-17A, which promotes activation of the phagocytosis respiratory burst response and indirect activation of CD8+ T cells(23, 24). Then, we verified the production of IL-17A in the serum of infected mice at both 15 and 150 d.p.i. There was no difference in the production of this cytokine between the treated groups (Fig S4). Although, recent report showed that Th17 are an important impact on protection against *T cruzi* infection, the classical immune protection is based on Th1 response (24). Proinflammatory cytokine production, such IL-12, TNF and IFN-γ are required to activate T lymphocytes, macrophage and other cells, resulting in parasite control (25–27). Surprisingly, we observed an increase of IFN-γ production in 4-Cl -infected treated mice, higher than mice treated wih Bz(-) but lower than those treated with saline (Fig. 6A). This high production of IFN-γ remained constant until chronicity of the disease, at levels similar to the optimal dose of Bz (Bz+) (Fig. 6B). This fact may suggest that the 4-Cl may modulate the immune response at the beginning of infection.

Fig. 6. **Treatment with 4-Cl increases the systemic production of IFN-γ in animals infected with *T. cruzi*.** IFN-γ was measured by ELISA in the serum of Balb/C mice infected and treated with Bz(-) (2.8 mg/kg/day) and/or 4-Cl (2.8 mg/kg/day) and Bz(+) (100 mg/kg/day). (A) Acute phase – 15 d.p.i. (n = 5) and (B) chronic phase – 150 d.p.i. (n = 7). Student's t test and nonparametric data were compared with the Mann-Whitney U test. Significant differences compared to the control or Bz(-) are denoted by $^{\&}p<0.05$ and $^{*}p<0.05$, respectively.

In silico binding study of 4-Cl

The activity of the immune system induced by 4-Cl is substantial; however, 4-Cl is considered a hybrid molecule, and the presence of two or more mechanisms of action for this molecule is not surprising. Therefore, the investigation of other possible targets inside *T. cruzi* is recommended (28). Since thiosemicarbazones are known to inhibit the *T. cruzi* protease cruzain, an enzyme that has essential functions for parasite survival as discussed above, a molecular docking simulation was performed with this enzyme to identify its possible role as a target of 4-Cl in the parasite. The predicted binding mode of the highest ranked compound with cruzain is presented in Fig. 6. It shows the electrostatic (Fig. 7A) and the hydrophobic (Fig. 7B) cruzain surfaces interacting with 4-Cl. The binding pocket core is primarily composed of basic and hydrophobic amino acid residues. The compound from this study strongly interacts with thirteen cruzain hydrophobic residues as shown in Fig. 7C. The binding mode of 4-Cl was compared with those of two other inhibitors whose crystal structures with cruzain were determined by X-ray crystallography and show interactions in the same pocket (29, 30) (Fig S5). Many basic and hydrophobic amino acid residues from cruzain were shown to be important for *in vivo* regulation of cruzain activity (29). No secondary binding site was found by the docking simulations with the studied compound (Fig S6), although two

297 uncharacterised cruzain binding sites were found in a recent theoretical investigation
298 (31).

299

300 **Fig. 7.** Molecular docking results of the complex formed by the cruzain protease with 4-
301 Cl bound to the enzyme active site. A) Electrostatic surface representation of the
302 complex. B) Hydrophobic surface representation of the complex. C) Cartoon
303 representation of cruzain with the compound in green. D) Hydrophobic residues from
304 the cruzain binding pocket interacting with 4-Cl. Charged residues are coloured blue
305 (positive) or red (negative), and hydrophobicity ranges from high (red) to low (white).

306
307 Another notable interaction is with the cysteine sulphur (SG) atom from residue Cys25,
308 which is approximately 3.0 Å away from the S and Au atoms of [Au(Hdamp)($L1^4$)]Cl,
309 as presented in Figure 8. The active site cysteine Cys25 was previously shown to
310 interact via a hydrogen bond with a hydroxymethyl ketone inhibitor and to be a mode of
311 inhibition of cruzain (32). In fact, SG from Cys25 is oriented in the direction of the Au
312 atom from [Au(Hdamp)($L1^4$)]Cl, which suggests formation of a possible covalent bond
313 with the compound. The sulphur atom from the cruzain active site, residue Cys25, was
314 previously reported to be covalently bound to the Z-Phe-Ala-FMK inhibitor (32) and
315 many others inhibitors as well, especially vinyl sulfone derivatives (12, 33, 34).
316 Synthesis and in vitro evaluation of gold(I) thiosemicarbazone complexes for
317 antimalarial activity (34). New experimental data from the crystallization of this
318 compound inside cruzain are necessary to confirm how 4-Cl is bound to cruzain.
319 Although the compound is stable in solution, we cannot determine from the current data
320 if the effect is directly caused by this molecule or its metabolites. In addition, the
321 interaction with other enzymes from *T. cruzi* cannot be eliminated.

322

323 **Fig. 8.** The cruzain active site cysteine Cys25 is predicted to be ~3.0 Å away from the
324 S2 and Au atoms of 4-Cl.

325
326 **Discussion**

327 The 4-Cl treatment on *T. cruzi*-infected mice is an interesting treatment because its low
328 concentration, stability and when used, in a very short-term treatment could
329 significantly improve the survival of the animals. Besides that, the synthesis is quite
330 simple, occurring at room temperature in a short period of time, and has an excellent
331 yield (almost 90%). The compound is easily crystallised, which leads to a high purity.
332 Therefore, although it is a gold compound, the costs for preparation do not limit its use.
333 Furthermore, the ESI^+ MS spectrum shows an exclusive $[M]^+$ molecular ion peak with
334 no evidence for the formation of gold(I) compounds, a common finding for gold(III)
335 thiosemicarbazone derivatives. Even when incubated in aqueous solution or in the
336 presence of a reducing agent, such as glutathione, for 24 h at 37 °C, the compound did
337 not show changes in retention time on HPLC (8). This finding is consistent with the
338 high stability of 4-Cl, which is a consequence of the organometallic Hdamp moiety.
339 These characteristics, together with its promising biological activity, are necessary for a
340 drug candidate.

341 In very low dosage, 4Cl was shown to be significantly selective against both
342 tryposmastigote and amastigote forms of parasite *in vitro* but presented a reduction of
343 nearly 60% of parasitemia, *in vivo,* without alteration in the parasitic load when
344 compared to the same dosage of Bz(-) in the acute phase of infection. This apparent
345 inefficiency in reducing cardiac parasitism, at the onset of infection, may be justified by
346 intrinsic distribution characteristic of the strain. The Y strain is known for its
347 fagotropism at the beginning of infection, reaching organs such as the spleen, liver and
348 bone marrow, and later moves to the muscle cells from the skeletal muscle and heart

(35). The quantification of PCR parasitism in the heart at 15 d.p.i. did not reflect the animal´s parasitic burden in the organism. Consequently, it is difficult to conclude that all parasites quantified in the blood were reallocated to the heart. This temporal synchrony became clearer when we observe the cardiac parasitism in the chronic phase in which the 4-Cl treatment was more efficient than the full dosage of Bz (Bz+) in eliminating the parasites of heart demonstrating an intrinsic 4-Cl ability to protect the mice of infection.

One of the aggravating factors of the therapy with Bz are its side effects. At a dose of 100 mg/kg, Bz is hepatotoxic due to high levels of reactive metabolites that are directly generated during Bz metabolism (6, 20, 36). The toxicity of Bz is higher than the damage caused by *T. cruzi* infection. The combination of infection plus Bz treatment by itself increases the levels of both AST and ALT (20). There are no reports showing ALT levels in chronic-phase Bz-treated mice. Our report is the first to demonstrate this small recovery of hepatic lesions after Bz treatment in the acute phase of *T. cruzi* infection. Additionally, Santra et al. (2000) (37) showed that 6-month-old Balb/C mice had baseline levels of 24.30 U/L. These values are very similar to values found for 4-Cl-treated mice after 150 d.p.i. (~20 U/L) that showed a higher reduction of the ALT enzyme than that for the clinical dose of Bz(+) (Fig. 5B), indicating that the 4-Cl treatment is not toxic to the liver. In addition, the toxicity demonstrated during the end of the 4-Cl treatment (50 U/L) was likely due to the parasite burden present in the acute phase of infection. Consistent with these findings, the AST concentration in the serum of C57BL/6 mice, which are resistant to *T. cruzi* infection, is 50 U/L after 15 d.p.i (20), confirming that the little hepatotoxicity found after the treatment may be due to infection and not directly due to some metabolite of the compound.

373 *T. cruzi* shows preferential tropism for the muscle tissue. Locally, the presence of
374 parasites recruits inflammatory cells to control and eliminate parasitaemia and tissue
375 parasitism, but eventually, this event leads to death caused by *T. cruzi*-induced
376 myocarditis (38). Within the first 15 days of treatment, the reduction of both
377 parasitaemia and cardiac parasitism (Fig. 3A and B) was reflected in the decrease in
378 blood CK-MB levels after 4-Cl treatment (Fig. 5C). However, this reduction was not
379 sufficient to reach the basal levels of uninfected mice, indicating that infection itself or
380 the recruitment of inflammation, for example, may damage cardiomyocytes during the
381 acute phase of the disease. This reduction is substantial over the time, and it was shown
382 to be significant compared with that of Bz(+). Together, these results emphasise the
383 protective effect of 4-Cl during the acute *T. cruzi* infection without causing toxicity to
384 the mammalian organism.
385 The protection against *T. cruzi* infection is accomplished by an efficient immune
386 response of Th1 profile cells, the major producers of IFN-γ cytokines, and more
387 recently by effector CD4+ T helper lymphocytes, called Th17 cells, which primarily
388 produce interleukin 17 (IL-17). Together, these immune responses are essential for
389 controlling the parasitism and cardiac inflammation during the infection (23). However,
390 excess Th1-biased CD4+ T cells orchestrate a CD8+T cell response that causes tissue
391 destruction and fibrosis (39, 40). Consequently, a balance of this response is crucial for
392 survival of the organism during the infection (39). As shown in this study, the 4-Cl
393 treatment reduced the parasitic burden (Fig. 3), which decreased antigenic exposure and
394 reduced the recruitment of immune cells (41). Therefore, we expected a reduction of
395 IFN-γ production in the serum of treated mice 15 d.p.i. Surprisingly, the gold(III)
396 complex increased the IFN-γ production compared to that in Bz(+)-treated mice, but it
397 was significantly reduced compared with that of the saline group (Fig. 6A) at the early

stage of infection. In accordance with our data, during the acute phase, the intense parasite burden activates the murine immune system to produce approximately 2000 pg/µL of IFN-γ in the Balb/C (23) serum and 200 pg/µL in C57BL/6 mice (20, 42). Novaes et al. (20) showed that after Bz treatment, the IFN-γ levels were reduced by half in C57BL/6 mice. Therefore, a reduction in the levels of this cytokine is expected after Bz treatment. The acute phase of *T. cruzi* infection is marked by an intense inflammatory infiltrate that is reduced when the disease reaches the chronic stage.

Throughout the infection, the cytokine levels were reduced to normal levels comparable to those of the Bz(+) group (Fig. 6B). At this late stage, there is a significant amount of CD8 T cells producing IFN-γ (43) and perforin (44), which are responsible for the maintenance of high levels of this cytokine (44, 45), while secreted perforin leads to late lesions in muscle fibres and cardiac alterations (44). Although treatment with Bz reduces the parasitic burden and, consequently, the inflammatory infiltrate, the action of Bz remains still dependent of the amount of IFN-γ produced. When IFN-γ knockout mice were treated with Bz, they were more susceptible than those treated with posoconazole (46). Our results contrasted to the amount of IFN-γ induced by Bz (Fig. 6). The IFN-γ production was high in the acute phase and decreased in the chronic stage. The early increase of this cytokine may be important to combat the parasites during the acute phase, since IFN-γ acts directly on macrophages, increasing their trypanocidal capacity (47). However, this change may also damage the cardiac tissue, as shown by the elevated levels of CK-MB in the serum of infected and 4-Cl-treated mice. In addition, the reduction of the parasite nests in the cardiac tissue (Fig. 3D) should be reflected in the reduction of IFN-γ production at the chronic stage of 4-Cl-treated mice. The high levels of IFN-γ at the beginning of the infection may be protective if combined with the other parameters, such as reduction of the parasitic burden, cardiac and hepatic

423 protection and mouse survival as long as that in the Bz(+) group. However, it may also
424 damage the cardiac tissue, as shown by the elevated CK-MB in the serum of infected
425 and 4-Cl-treated mice. Together, these results suggest that treatment with 4-Cl may act
426 in the immune system by promoting the release of IFN-γ, which acts directly on parasite
427 death.
428 Similarly, treatment with an equal concentration of Bz was not able to produce these
429 improvements. As demonstrated by our in silico data, the complex gold(III)-
430 thiosemicarbazone probably interacts with cruzain, a major cysteine protease of *T. cruzi*
431 crucial to multiplication and amastigote survival of *T. cruzi* (8, 10),which can be shown
432 by its direct action on the amastigote and trypomastigote forms of *T. cruzi* in both the Y
433 strain and the Tulahuen strain (8). In addition, the lower levels of tissue parasitism in
434 both skeletal muscle and heart of 4-Cl-treated mice were followed by a reduction of
435 cardiac and hepatic tissue damage, showing a protective effect of this compound.
436 Curiously, 4-Cl could increase the production of systemic IFN-γ, which indirectly kills
437 the parasite by the recruitment of an efficient immune response against *T. cruzi* (48).
438 Therefore, the gold(III) complex appears to act on two different pathways of parasite
439 death. As predicted by our previous study (8), this complex may have multiple targets
440 and mechanisms of action by affecting different biological functions in the parasite.
441 Future studies will reveal how the 4-Cl complex modulates the immune response:
442 whether the increase of IFN-γ can activate macrophages to produce nitric oxide, the
443 most classic form of *T. cruzi* death by immune system (40); if it inhibits other parasite
444 enzymes, such as TcOYE (49, 50); or if this complex produces intracellular reactive
445 oxygen species, which are known to cause damage to *T. cruzi*. In any case, 4-Cl was
446 shown to be a potential candidate for the treatment of Chagas disease.

447 **Conclusion**

448 The gold(III) complex 4-Cl was shown to be effective in directly killing the parasite in
449 both the trypomastigote and amastigote forms of *T. cruzi*. The *in vivo* assays
450 demonstrated that 4-Cl reduces parasitaemia and tissue parasitism at a very low dose in
451 addition to protecting the liver and heart from tissue damage, leading to the survival of
452 100% of the 4-Cl-treated mice during the acute phase. The same effect has been
453 observed only when the mice were treated with the maximum dose of Bz. During the
454 acute phase, we observed a specific increase of systemic IFN-γ, a classical cytokine for
455 protection of the organism during Chagas disease. Interestingly, during the chronic
456 phase, the production of this cytokine returns to the same levels as that of the Bz(+)
457 treatment, which indicates that 4-Cl can modulate the immune response during the
458 treatment period. Theoretical studies (molecular docking) suggest that 4-Cl could
459 interact with cruzain via hydrophobic interactions and that it might react with Cys25, a
460 residue commonly found to be covalently bound to many other cruzain inhibitors.
461 Future studies on the biochemical and metabolic pathways are necessary to further
462 elucidate the anti-*T. cruzi* mechanism of action of this drug candidate. However, from
463 the data presented thus far, 4-Cl appears to act on two different pathways. This study
464 has confirmed that the organometallic gold(III)-thiosemicarbazone complex 4-Cl may
465 be a new candidate for the development of novel anti-chagasic drugs and may accelerate
466 the investigations based on metallotherapeutics for the treatment of Chagas disease.
467

468 **Materials and Methods**

469

470 **Reagents and supply**

471 The synthesis of 4-Cl has been described previously (8). Benznidazole was purchased
472 from Sigma-Aldrich (used as a reference drug). RPMI medium 1640 (with or without

phenol red) supplemented with 5% bovine fetal serum (GIBCO, Grand Island, NY, USA), 100 IU mL^{-1} penicillin G, and 100 mg mL^{-1} streptomycin (Gibco-BRL, Grand Island, NY, USA) was used. Dimethyl sulfoxide (DMSO) was obtained from Sigma-Aldrich Chemicals, Co. (St. Louis, MO, USA).

T. cruzi stocks

All the procedures and animal protocols were conducted in accordance with the National Brazilian College of Animal Experimentation (COBEA) and approved by the Commission of Ethics in Animal Research of the University of São Paulo, Medical School of Ribeirão Preto (CETEA) - Protocol number 100/2014.

For the *in vitro* experiments, the LLC-MK2 cells were infected with bloodstream trypomastigote forms, which were derived from previously infected Swiss mice. For the *in vivo* experiments, mice were intraperitoneally inoculated with 2000 bloodstream trypomastigote forms, also derived from previously infected Swiss mice.

In vitro evaluation of trypanocidal activity against the trypomastigote and amastigote forms

Trypomastigote forms of the *T. cruzi* Y strain were obtained from infected LLC-MK2 cell culture and suspended at a concentration of 6.5×10^6 parasites/mL in RPMI 1640 liquid medium without phenol red. They were cultured in flat-bottom 96-well plates at various concentrations of Bz or 4-Cl at 37 °C for 24 h. The viability of the parasites was determined by counting the motile parasites in a Neubauer chamber as previously described (7, 51). The concentration of the compound corresponding to 50% trypanocidal activity in trypomastigote was expressed as the IC_{50Try}.

For evaluation of the trypanocidal activity of the compound against the amastigote forms of the *T. cruzi* Y strain, differentiated bone marrow macrophages (BBMs) were used as previously described (52), and femurs were obtained from 6-8-week-old C57BL/6 mice. Cells were seeded in non-tissue culture-treated Optilux Petri dishes (BD Biosciences) and incubated at 37 °C in a 5% CO_2 atmosphere. Four days after seeding the cells, an extra 10 mL of fresh R20/30 was added per plate and incubated for an additional 3 days. The supernatants were discarded, and the attached cells were washed with 10 mL of sterile PBS to obtain the BBMs. The macrophages were detached by gently pipetting the PBS. The cells were centrifuged at 200× g for 5 minutes and resuspended in 10 mL of BBM cultivation media (R10/5). The cells were counted, seeded (5.0×10^4 cells/well) and cultivated in tissue culture plates for 24 hours. After 24 hours, the BBMs were infected with trypomastigote forms (1×10^5 parasites/well) for 16 h. The cells were washed to remove parasites in the supernatant and incubated with Bz or 4-Cl for an additional 24 h at 37 °C. Cells were stained with Giemsa dye and evaluated by optical microscopy [21]. Trypanocidal activity was determined by counting the parasites/cell in at least 200 cells.

In vitro evaluation of the cytotoxicity in BBMs

BBMs were assessed by the colorimetric method [3-4,5-dimethylthiazol-2-yl) 2,5-diphenyl tetrazoyl bromide] (MTT) (53). BBMs were suspended at a concentration of 5.0×10^5 cells/mL in RPMI medium without phenol red supplement with 5% fetal bovine and incubated for 24 hours in 96-well cell culture plates. After this incubation period, the Bz and Gold(III) complex were added at serially diluted concentrations ranging from 125.0 to 1.95 µM. The cells were incubated for 24 hours at 37 °C. After incubation, the medium was removed, and fresh culture medium containing 50 µM of

MTT (2.5 mg mL^{-1}) diluted in phosphate buffered (PBS) was added. The precipitated blue MTT formazan was dissolved in 50 µL of DMSO, and the absorbance was measured at 570 nm in a VARIAN CARY-50 multiwell MPR plate reader. Cell viability was expressed as the percentage of absorption values in treated cells compared with untreated (control) cells. The concentration of the compound corresponding to 50% cytotoxicity in the BBMs was expressed as the CC_{50BBMs}.

Animal inoculum and treatment

Balb/c female mice (4 – 6 weeks old) with an average weight of approximately 20 ± 3 g were used to determine the trypanocidal activity of the compounds in the acute phase of Chagas disease. All animals were kept under the same conditions, receiving water and food ad libitum. Animals were infected intraperitoneally with 2.0 x 10^3 blood trypomastigote forms of the *T. cruzi* Y strain (7, 51). The mice were orally treated, and treatment started at five days post-infection (d.p.i) for 10 consecutive days. The daily doses of the compounds tested were 2.8 mg/kg/day of 4-Cl, 2.8 mg/kg/day of Bz(-), and 100 mg/kg/day of Bz(+). Bz(+) was used as a positive control in the study (7). For analysis of the acute stage of infection, the animals were euthanised after 15 d.p.i. The mice that survived the acute phase were followed for 150 d.p.i., and their organs and serum were removed and stored at -80° C for further analysis.

Parasitaemia and survival assessment

Parasitaemia was analysed on alternate days from the 5^{th} d.p.i. To this end, 5 µL of fresh blood was collected from the animal tail. The count in 100 fields was performed via direct observation under a light microscope (54). The survival was determined by daily

547 inspection for more than 150 consecutive days in which mice were weighed to monitor
548 the effects of the infection.
549
550 **Quantification of cardiac and hepatic injury**
551 The blood of infected mice was collected by cardiac puncture and centrifuged for 10
552 minutes at 12000 g. Then, the serum was removed and stored at minus 4 °C until
553 performance of biochemical assays. The cardiac lesions of mice infected with *T.*
554 *cruzi*, treated or not, were assessed by measuring the serum creatine kinase-MB
555 (CK-MB) levels at 15 and 150 d.p.i. The CK-MB levels were measured using a CK-
556 MB kit (LABTEST, Brazil), as previously described (55). Absorbance was
557 measured on a microplate spectrophotometer (EMAX Molecular Devices
558 Corporation, California, EUA). The colour produced from this reaction was
559 measured at a wavelength of 340 nm; the results are expressed in U/L. The hepatic
560 damage was evaluated by measuring Aspartate aminotransferase (AST) and alanine
561 aminotransferase (ALT) using a LABTEST system (Brazil), according to the
562 manufacturer's instructions. The colour produced by this reaction was measured at a
563 wavelength of 340 nm. The results are expressed in U/L.
564
565 **Histological analysis**
566 Groups of five mice were euthanised at 15 and 150 d.p.i., and the hearts were fixed in
567 paraffin for histological analysis. For analysis of amastigote nests via light optical
568 microscopy (Axioskop 40), tissues were sectioned at a 5-µm thickness, stained with
569 haematoxylin-eosin (H&E) and examined under a light microscope with 40 times
570 magnification. Each tissue section was imaged 10 times and used to analyse the
571 amastigote nests.

572

573 **Quantitative real-time polymerase chain reaction (qPCR)**

574 The qPCR technique was used to determine the amount of parasite DNA in the tissues
575 collected from infected and treated animals. The DNA was purified from 10 mg of heart
576 tissue using Wizard® Genomic DNA Purification (Promega), according to the
577 manufacturer's instructions. Each qPCR reaction contains 20 ng of genomic DNA, 0.3
578 µM of the specific primers of *T. cruzi* (TCZ-F 5′-GCTCTTGCCCACAMGGGTGC-3′
579 (M=A or C) and TCZ-R 5′-CCAAGCAGCGGATAGTTCAGG-3″(56)), which amplify
580 a 182 bp product, 7.6 µL GoTaq qPCR Master Mix® (Promega), and H_2O to a final total
581 volume of 15 µL. Reactions were performed using the StepOnePLus™ Real-Time
582 qPCR System (Applied Biosystems, Foster City, CA, USA). The cycle programme was
583 95 °C for 10 minutes, followed by 50 cycles of three steps, denaturation at 95 °C for 15
584 seconds, annealing at 55 °C for 30 seconds, and amplification at 72 °C for 15 seconds.
585 The melting phase was performed at 95 °C for 15 seconds and 60 °C for 60 seconds,
586 followed by a 0.3 °C ramp and 95 °C for 15 seconds. During the melting phase, the
587 acquisition setting was set at step. The data were analysed with StepOne Software
588 version 2.2.2.

589

590 **Cytokine quantification by ELISA**

591 For analysis of cytokine production in the serum of treated-infected mice, blood was
592 collected by cardiac puncture and centrifugated at 12000 g for 10 minutes. The serum
593 was collected and frozen at -20 °C. The ELISA sets were IL-17A and IFN-γ (R&D,
594 Minneapolis, MN, USA). All technical procedures were performed according to the
595 manufacturer´s instruction. The limits of sensitivity for different assays were as follows:
596 15 pg/mL for IL-17A and 31.2 pg/mL for IFN-γ.

Docking studies

The X-ray crystallographic data of the cruzain protease was extracted from the Protein Data Bank (18) (PDB, code 1AIM). Molecular docking simulations were performed with Genetic Optimization for Ligand Docking (GOLD) suite version 5.5. The complete protocol is presented in the **Supporting Information** section.

Statistical analysis

The statistical analyses are representative of the mean ± SEM of three independent experiments, (n=5), using Student's t test and Mann-Whitney *post test* analysis. Data were considered significant when $p<0.05$. (*) indicates differences compared to the PBS-treated mice and (&) differences from the Bz(+)-treated group. All analyses were performed using PRISM 5.0 software (GraphPad, San Diego, CA, US).

Acknowledgements

The authors gratefully acknowledge the technical assistance of Cristiane Maria Milanezi and Wander Ribeiro. We also thank Rubilan Carneiro Quionero for supervising the animal facility as well as providing all animals used in this study. The research leading to these results received funding from CAPES and CRID, Center for Research in Inflammatory Disease.

References

1. WHO | Chagas disease (American trypanosomiasis). WHO.

2. Molyneux DH, Savioli L, Engels D. 2017. Neglected tropical diseases: progress towards addressing the chronic pandemic. Lancet Lond Engl 389:312–325.

620 3. Guedes PMM, Silva GK, Gutierrez FRS, Silva JS. 2011. Current status of Chagas
621 disease chemotherapy. Expert Rev Anti Infect Ther 9:609–620.

622 4. Viotti R, Alarcón de Noya B, Araujo-Jorge T, Grijalva MJ, Guhl F, López MC,
623 Ramsey JM, Ribeiro I, Schijman AG, Sosa-Estani S, Torrico F, Gascon J, Latin
624 American Network for Chagas Disease, NHEPACHA. 2014. Towards a paradigm
625 shift in the treatment of chronic Chagas disease. Antimicrob Agents Chemother
626 58:635–639.

627 5. Bermudez J, Davies C, Simonazzi A, Real JP, Palma S. 2016. Current drug
628 therapy and pharmaceutical challenges for Chagas disease. Acta Trop 156:1–16.

629 6. Urbina JA. 2010. Specific chemotherapy of Chagas disease: relevance, current
630 limitations and new approaches. Acta Trop 115:55–68.

631 7. Carneiro ZA, Maia PI da S, Sesti-Costa R, Lopes CD, Pereira TA, Milanezi CM,
632 da Silva MAP, Lopez RFV, Silva JS, Deflon VM. 2014. In vitro and in vivo
633 trypanocidal activity of H2bdtc-loaded solid lipid nanoparticles. PLoS Negl Trop
634 Dis 8:e2847.

635 8. Maia PI da S, Carneiro ZA, Lopes CD, Oliveira CG, Silva JS, Albuquerque S de,
636 Hagenbach A, Gust R, Deflon VM, Abram U. 2017. Organometallic gold(III)
637 complexes with hybrid SNS-donating thiosemicarbazone ligands: cytotoxicity and
638 anti-Trypanosoma cruzi activity. Dalton Trans 46:2559–2571.

639 9. Lepesheva GI. 2013. Design or screening of drugs for the treatment of Chagas
640 disease: what shows the most promise? Expert Opin Drug Discov 8:1479–1489.

641 10. Doyle PS, Zhou YM, Hsieh I, Greenbaum DC, McKerrow JH, Engel JC. 2011.
642 The Trypanosoma cruzi Protease Cruzain Mediates Immune Evasion. PLOS
643 Pathog 7:e1002139.

644 11. da Silva Maia PI, Deflon VM, Abram U. 2014. Gold(III) complexes in medicinal
645 chemistry. Future Med Chem 6:1515–1536.

646 12. Rettondin AR, Carneiro ZA, Gonçalves ACR, Ferreira VF, Oliveira CG, Lima
647 AN, Oliveira RJ, de Albuquerque S, Deflon VM, Maia PIS. 2016. Gold(III)
648 complexes with ONS-Tridentate thiosemicarbazones: Toward selective
649 trypanocidal drugs. Eur J Med Chem 120:217–226.

650 13. Tostes Júnior S, Lopes ER, Pereira FE, Chapadeiro E. 1994. [Human chronic
651 chagasic myocarditis: quantitative study of CD4+ and CD8+ lymphocytes in
652 inflammatory exudates]. Rev Soc Bras Med Trop 27:127–134.

653 14. de Araújo-Souza PS, Hanschke SCH, Viola JPB. 2015. Epigenetic control of
654 interferon-gamma expression in CD8 T cells. J Immunol Res 2015:849573.

655 15. Tarleton RL, Sun J, Zhang L, Postan M. 1994. Depletion of T-cell subpopulations
656 results in exacerbation of myocarditis and parasitism in experimental Chagas'
657 disease. Infect Immun 62:1820–1829.

658 16. Luckheeram RV, Zhou R, Verma AD, Xia B. 2012. $CD4^+$T cells: differentiation
659 and functions. Clin Dev Immunol 2012:925135.

660 17. Gowda S, Desai PB, Hull VV, Math AAK, Vernekar SN, Kulkarni SS. 2009. A
661 review on laboratory liver function tests. Pan Afr Med J 3:17.

662 18. Sadok Menna-Barreto RF, Belloze KT, Perales J, Silva FP. 2014. Proteomic and
663 bioinformatic analysis of Trypanosoma cruzi chemotherapy and potential drug
664 targets: new pieces for an old puzzle. Curr Drug Targets 15:255–271.

665 19. Veloso VM, Guedes PMM, Andrade IM, Caldas IS, Martins HR, Carneiro CM,
666 Machado-Coelho GLL, de Lana M, Galvão LMC, Bahia MT, Chiari E. 2008.
667 Trypanosoma cruzi: blood parasitism kinetics and their correlation with heart
668 parasitism intensity during long-term infection of Beagle dogs. Mem Inst Oswaldo
669 Cruz 103:528–534.

670 20. Novaes R, Santos E, Cupertino M, Bastos D, Oliveira J, V Carvalho T, Neves M,
671 Oliveira L, Talvani A. 2015. Trypanosoma cruzi infection and benznidazole
672 therapy independently stimulate oxidative status and structural pathological
673 remodeling of the liver tissue in mice. Parasitol Res 114.

674 21. Sathler-Avelar R, Vitelli-Avelar DM, Massara RL, de Lana M, Pinto Dias JC,
675 Teixeira-Carvalho A, Elói-Santos SM, Martins-Filho OA. 2008. Etiological
676 treatment during early chronic indeterminate Chagas disease incites an activated
677 status on innate and adaptive immunity associated with a type 1-modulated
678 cytokine pattern. Microbes Infect 10:103–113.

679 22. Sathler-Avelar R, Vitelli-Avelar DM, Elói-Santos SM, Gontijo ED, Teixeira-
680 Carvalho A, Martins-Filho OA. 2012. Blood leukocytes from benznidazole-treated
681 indeterminate chagas disease patients display an overall type-1-modulated
682 cytokine profile upon short-term in vitro stimulation with Trypanosoma cruzi
683 antigens. BMC Infect Dis 12:123.

684 23. da Matta Guedes PM, Gutierrez FRS, Maia FL, Milanezi CM, Silva GK, Pavanelli
685 WR, Silva JS. 2010. IL-17 produced during Trypanosoma cruzi infection plays a
686 central role in regulating parasite-induced myocarditis. PLoS Negl Trop Dis
687 4:e604.

688 24. Cai CW, Blase JR, Zhang X, Eickhoff CS, Hoft DF. 2016. Th17 Cells Are More
689 Protective Than Th1 Cells Against the Intracellular Parasite Trypanosoma cruzi.
690 PLoS Pathog 12.

691 25. Fuenmayor C, Higuchi ML, Carrasco H, Parada H, Gutierrez P, Aiello V,
692 Palomino S. 2005. Acute Chagas' disease: immunohistochemical characteristics of
693 T cell infiltrate and its relationship with T. cruzi parasitic antigens. Acta Cardiol
694 60:33–37.

695 26. Aliberti JC, Cardoso MA, Martins GA, Gazzinelli RT, Vieira LQ, Silva JS. 1996.
696 Interleukin-12 mediates resistance to Trypanosoma cruzi in mice and is produced
697 by murine macrophages in response to live trypomastigotes. Infect Immun
698 64:1961–1967.

699 27. Michailowsky V, Silva NM, Rocha CD, Vieira LQ, Lannes-Vieira J, Gazzinelli
700 RT. 2001. Pivotal Role of Interleukin-12 and Interferon-γ Axis in Controlling
701 Tissue Parasitism and Inflammation in the Heart and Central Nervous System
702 during Trypanosoma cruzi Infection. Am J Pathol 159:1723–1733.

703 28. Duschak VG. 2016. Targets and Patented Drugs for Chemotherapy of Chagas
704 Disease in the Last 15 Years-Period. Recent Patents Anti-Infect Drug Disc 11:74–
705 173.

706 29. Gillmor SA, Craik CS, Fletterick RJ. 1997. Structural determinants of specificity
707 in the cysteine protease cruzain. Protein Sci Publ Protein Soc 6:1603–1611.

708 30. Ferreira RS, Simeonov A, Jadhav A, Eidam O, Mott BT, Keiser MJ, McKerrow
709 JH, Maloney DJ, Irwin JJ, Shoichet BK. 2010. Complementarity Between a
710 Docking and a High-Throughput Screen in Discovering New Cruzain Inhibitors. J
711 Med Chem 53:4891–4905.

712 31. Huang L, Brinen LS, Ellman JA. 2003. Crystal structures of reversible ketone-
713 Based inhibitors of the cysteine protease cruzain. Bioorg Med Chem 11:21–29.

714 32. McGrath ME, Eakin AE, Engel JC, McKerrow JH, Craik CS, Fletterick RJ. 1995.
715 The crystal structure of cruzain: a therapeutic target for Chagas' disease. J Mol
716 Biol 247:251–259.

717 33. Gomes Vital D, Arribas M, Henrique Goulart Trossini G. 2014. Molecular
718 Modeling and Docking Application to Evaluate Cruzain Inhibitory Activity by
719 Chalcones and Hydrazides. Lett Drug Des Discov 11:249–255.

720 34. Khanye SD, Smith GS, Lategan C, Smith PJ, Gut J, Rosenthal PJ, Chibale K.
721 2010. Synthesis and in vitro evaluation of gold(I) thiosemicarbazone complexes
722 for antimalarial activity. J Inorg Biochem 104:1079–1083.

723 35. Melo RC, Brener Z. 1978. Tissue tropism of different Trypanosoma cruzi strains. J
724 Parasitol 64:475–482.

725 36. Castro JA, de Mecca MM, Bartel LC. 2006. Toxic side effects of drugs used to
726 treat Chagas' disease (American trypanosomiasis). Hum Exp Toxicol 25:471–479.

727 37. Santra A, Maiti A, Das S, Lahiri S, Charkaborty SK, Mazumder DN. 2000.
728 Hepatic damage caused by chronic arsenic toxicity in experimental animals. J
729 Toxicol Clin Toxicol 38:395–405.

730 38. Marin-Neto JA, Simões MV, Rassi Junior A. 2013. Pathogenesis of chronic
731 Chagas cardiomyopathy: the role of coronary microvascular derangements. Rev
732 Soc Bras Med Trop 46:536–541.

733 39. Gutierrez FRS, Guedes PMM, Gazzinelli RT, Silva JS. 2009. The role of parasite
734 persistence in pathogenesis of Chagas heart disease. Parasite Immunol 31:673–
735 685.

736 40. Gutierrez FR, Mineo TW, Pavanelli WR, Guedes PM, Silva JS. 2009. The effects
737 of nitric oxide on the immune system during Trypanosoma cruzi infection. Mem
738 Inst Oswaldo Cruz 104:236–245.

739 41. Zinkernagel RM, Hengartner H. 2001. Regulation of the Immune Response by
740 Antigen. Science 293:251–253.

741 42. Marinho CR, D'Império Lima MR, Grisotto MG, Alvarez JM. 1999. Influence of
742 acute-phase parasite load on pathology, parasitism, and activation of the immune
743 system at the late chronic phase of Chagas' disease. Infect Immun 67:308–318.

744 43. Bustamante JM, Bixby LM, Tarleton RL. 2008. Drug-induced cure drives
745 conversion to a stable and protective CD8+ T central memory response in chronic
746 Chagas disease. Nat Med 14:542–550.

747 44. Silverio JC, de-Oliveira-Pinto LM, da Silva AA, de Oliveira GM, Lannes-Vieira J.
748 2010. Perforin-expressing cytotoxic cells contribute to chronic cardiomyopathy in
749 Trypanosoma cruzi infection. Int J Exp Pathol 91:72–86.

750 45. Cutrullis RA, Poklépovich TJ, Postan M, Freilij HL, Petray PB. 2011.
751 Immunomodulatory and anti-fibrotic effects of ganglioside therapy on the cardiac
752 chronic form of experimental Trypanosoma cruzi infection. Int Immunopharmacol
753 11:1024–1031.

754 46. Ferraz ML, Gazzinelli RT, Alves RO, Urbina JA, Romanha AJ. 2007. The Anti-
755 Trypanosoma cruzi activity of posaconazole in a murine model of acute Chagas'
756 disease is less dependent on gamma interferon than that of benznidazole.
757 Antimicrob Agents Chemother 51:1359–1364.

758 47. Reed SG. 1988. In vivo administration of recombinant IFN-gamma induces
759 macrophage activation, and prevents acute disease, immune suppression, and death
760 in experimental Trypanosoma cruzi infections. J Immunol Baltim Md 1950
761 140:4342–4347.

762 48. Kayama H, Takeda K. 2010. The innate immune response to Trypanosoma cruzi
763 infection. Microbes Infect 12:511–517.

764 49. Verdonk ML, Cole JC, Hartshorn MJ, Murray CW, Taylor RD. 2003. Improved
765 protein-ligand docking using GOLD. Proteins 52:609–623.

766 50. Gonçalves ACR, Carneiro ZA, Oliveira CG, Danuello A, Guerra W, Oliveira RJ,
767 Ferreira FB, Veloso-Silva LLW, Batista FAH, Borges JC, de Albuquerque S,
768 Deflon VM, Maia PIS. PtII, PdII and AuIII complexes with a thiosemicarbazone
769 derived from diacethylmonooxime: Structural analysis, trypanocidal activity,

770 cytotoxicity and first insight into the antiparasitic mechanism of action. Eur J Med
771 Chem.

772 51. Sesti-Costa R, Carneiro ZA, Silva MC, Santos M, Silva GK, Milanezi C, da Silva
773 RS, Silva JS. 2014. Ruthenium complex with benznidazole and nitric oxide as a
774 new candidate for the treatment of chagas disease. PLoS Negl Trop Dis 8:e3207.

775 52. Marim FM, Silveira TN, Jr DSL, Zamboni DS. 2010. A Method for Generation of
776 Bone Marrow-Derived Macrophages from Cryopreserved Mouse Bone Marrow
777 Cells. PLOS ONE 5:e15263.

778 53. Mosmann T. 1983. Rapid colorimetric assay for cellular growth and survival:
779 application to proliferation and cytotoxicity assays. J Immunol Methods 65:55–63.

780 54. Brener Z. 1962. [Observations on immunity to superinfections in mice
781 experimentally inoculated with Trypanosoma cruzi and subjected to treatment].
782 Rev Inst Med Trop Sao Paulo 4:119–123.

783 55. Maekawa M. 2012. Effect of the Inhibition of Mitochondrial Creatine Kinase
784 Activity on the Clinical Diagnosis of Suspected Acute Myocardial Infarction.
785 Open Clin Chem J 5:1–6.

786 56. Cummings KL, Tarleton RL. 2003. Rapid quantitation of Trypanosoma cruzi in
787 host tissue by real-time PCR. Mol Biochem Parasitol 129:53–59.

788 57. Berman HM, Westbrook J, Feng Z, Gilliland G, Bhat TN, Weissig H, Shindyalov
789 IN, Bourne PE. 2000. The Protein Data Bank. Nucleic Acids Res 28:235–242.

790

791 **Figures**

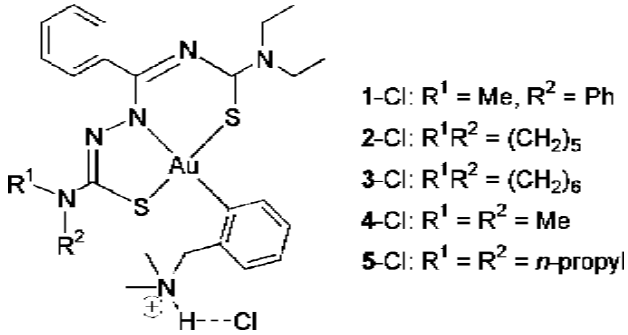

FIG 1. Organometallic gold(III) complexes containing hybrid *SNS*-donating thiosemicarbazone ligands $[Au^{III}(Hdamp)(L1)]Cl$ (Hdamp = dimethylammoniummethylphenyl) (Adapted from [9]).

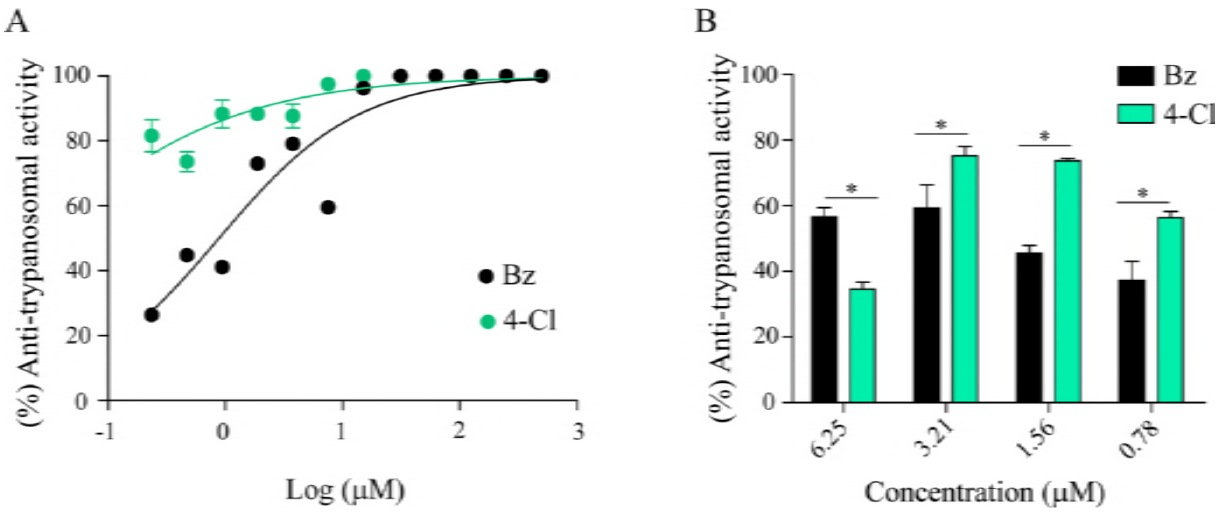

FIG 2. ***In vitro*** **trypanocidal activity of 4-Cl against the trypomastigote and amastigote forms of the Y strain of *T. cruzi*.** (A) Percentage of trypanocidal activity of 4-Cl and Bz against the Y strain of *T. cruzi* analysed by quantifying viable parasites 24 h post-treatment. (B) Macrophages derived from bone marrow were infected with the trypomastigote form of the Y strain of *T. cruzi*. After 24 hours of infection, the extracellular parasites were removed, and cells were infected with the amastigote forms and treated with 4-Cl or Bz. Assays were conducted using biological replicates.

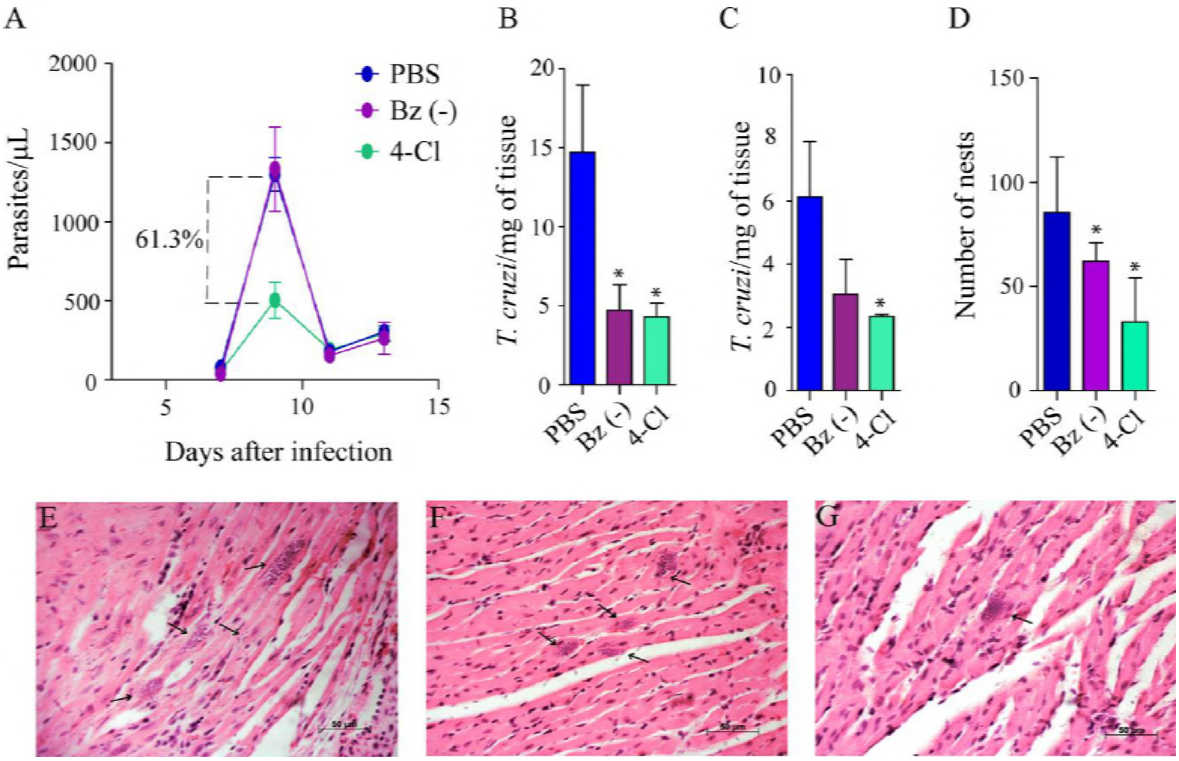

FIG 3. Parasitic burden in the blood and tissue of infected mice after treatment with 2.8 mg/kg/day of 4-Cl, 2.8 mg/kg/day of Bz(-) and 100 mg/kg/day of Bz(+) during the acute phase of infection. (A) Results indicated the decrease in parasitaemia of animals treated with 4-Cl. Parasitaemia was monitored on days 7, 9, 11 and 13 after infection. (B) Quantification of the parasite burden in cardiac tissues via real-time qPCR. The presence of *T. cruzi* in infected heart tissues of mice was analysed by qPCR 15 d.p.i. (C) Quantification of the parasite burden in skeletal tissues via real-time qPCR. The presence of *T. cruzi* in infected skeletal tissues of the mice was analysed by qPCR 15 d.p.i. (D) Number of amastigote nests in heart tissue. (E) Heart histological section of PBS-treated mice, (F) Bz(-)-treated mice and (G), 4-Cl-treated mice. Arrows indicate amastigote nests. The mean±SEM is shown and represents three independent experiments (n=5). Significance was defined when *$p \leq 0.05$.

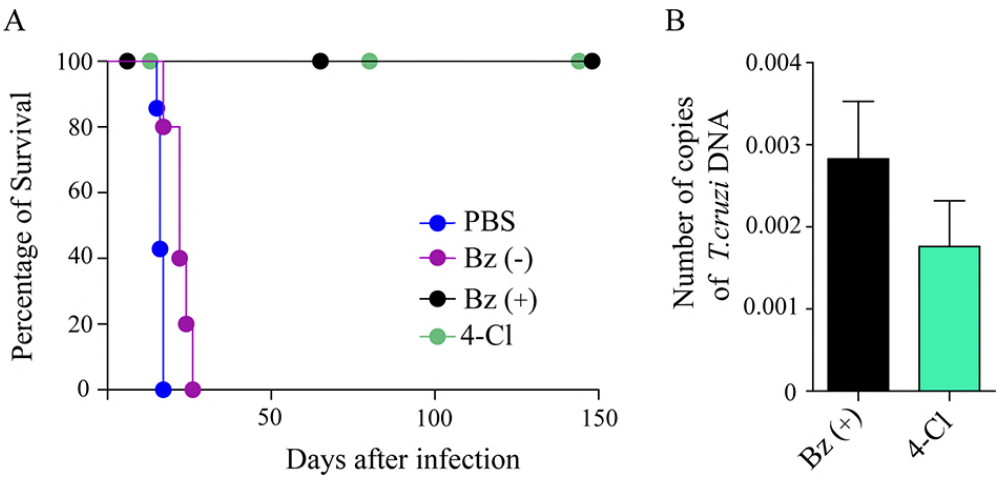

821

822

823 **FIG 4. The 4-Cl treatment protects the mice from *T. cruzi* infection.** (A) *T. cruzi*-
824 infected mice (n=7) were treated for 10 consecutive days, from the fifth day after
825 infection, with a Bz(-) concentration of 2.8 mg/kg, a Bz(+) concentration of 100 mg/kg
826 (positive control), a 4-Cl concentration of 2.8 mg/kg and PBS. The mice were followed
827 up for 150 days to evaluate survival. (B) *T. cruzi* DNA quantification in the hearts of
828 surviving mice (n=3).

829

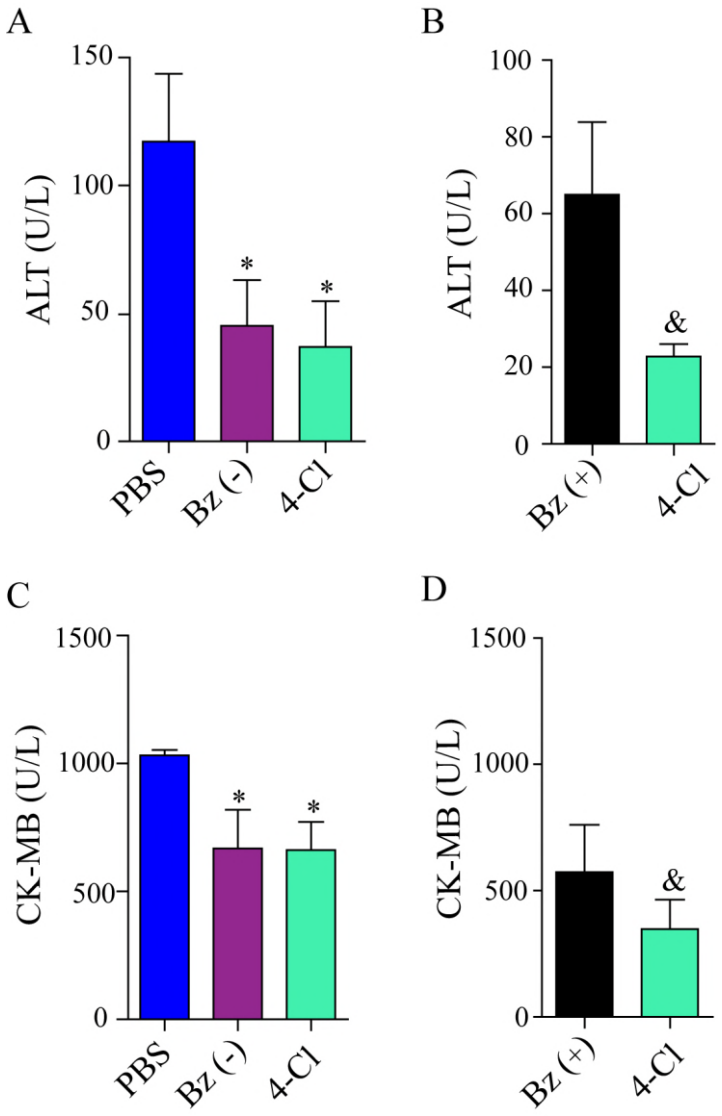

FIG 5. Liver and cardiac lesions of *T. cruzi*-infected mice after treatment with 4-Cl. Quantification of (A) Alanine Aminotransferase (ALT) 15 d.p.i. (acute phase), (B) Alanine Aminotransferase (ALT) 150 d.p.i. (chronic phase), (C) CK-MB (U/L) at 15 d.p.i. and (D) CK-MB (U/L) at 150 d.p.i. The data are represented as the mean ± SEM of three independent experiments, (n=5), using Student's t test and Mann-Whitney *post test* analysis. Data were considered significant when $p<0.05$. (*) indicates difference from PBS-treated mice and (&) differences from the Bz(+)-treated group.

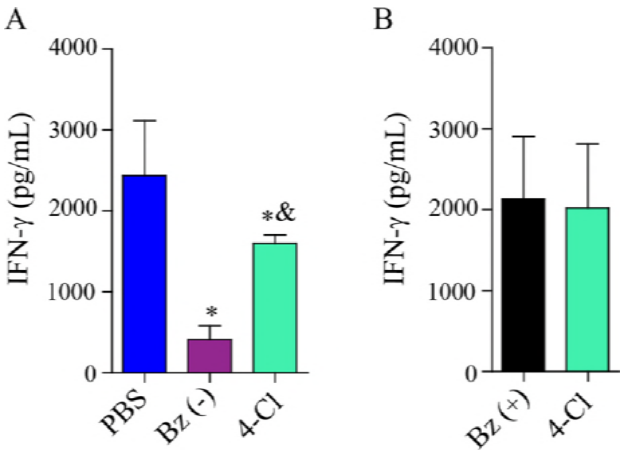

FIG 6. Treatment with 4-Cl increases the systemic production of IFN-γ in animals infected with *T. cruzi*. IFN-γ was measured by ELISA in the serum of Balb/C mice infected and treated with Bz(-) (2.8 mg/kg/day) and/or 4-Cl (2.8 mg/kg/day) and Bz(+) (100 mg/kg/day). (A) Acute phase – 15 d.p.i. (n = 5) and (B) chronic phase – 150 d.p.i. (n = 7). Student's t test and nonparametric data were compared with the Mann-Whitney U test. Significant differences compared to the control or Bz(-) are denoted by $^{\&}p<0.05$ and $^{*}p<0.05$, respectively.

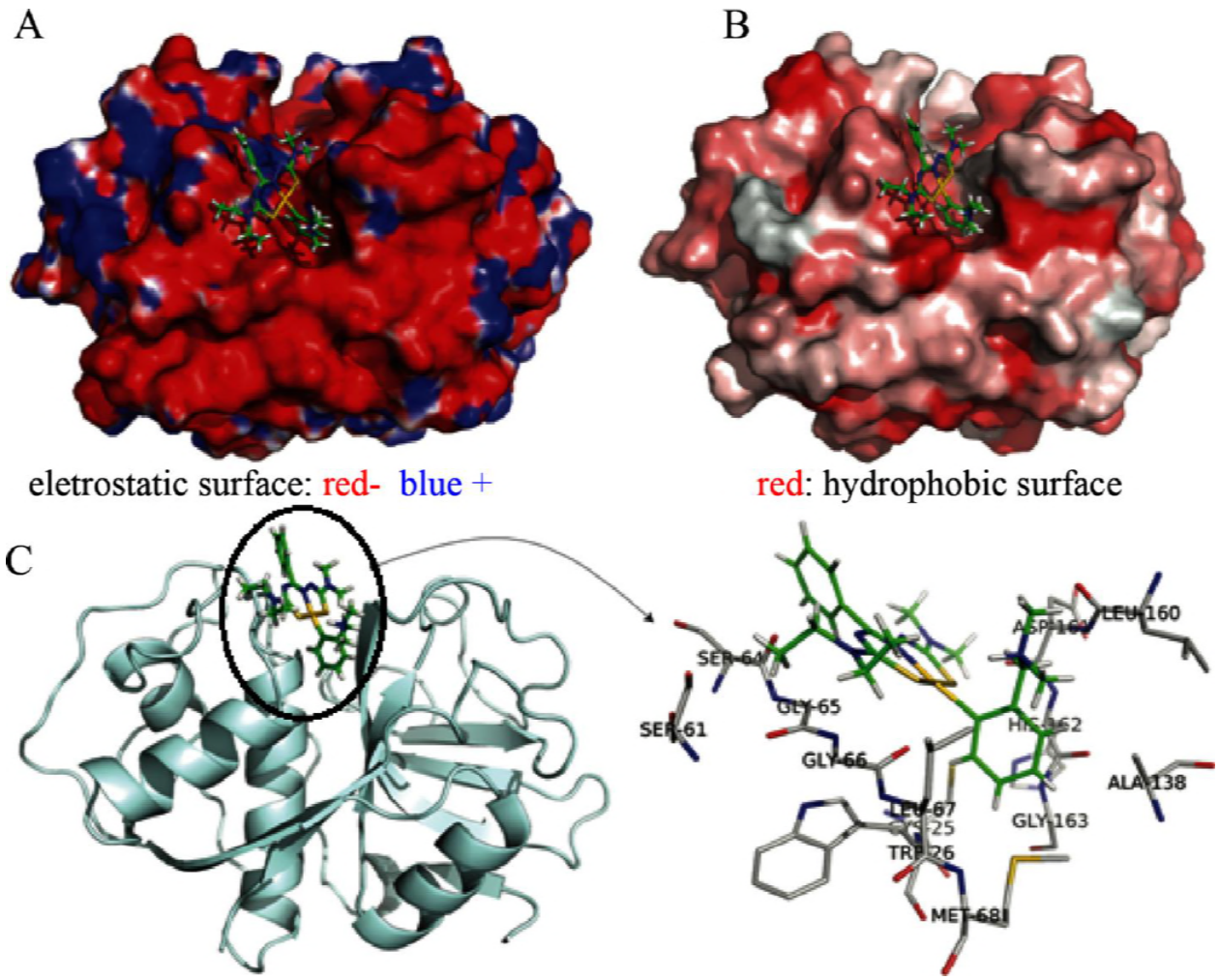

FIG 7. Molecular docking results of the complex formed by the cruzain protease with 4-Cl bound to the enzyme active site. A) Electrostatic surface representation of the complex. B) Hydrophobic surface representation of the complex. C) Cartoon representation of cruzain with the compound in green. D) Hydrophobic residues from the cruzain binding pocket interacting with 4-Cl. Charged residues are coloured blue (positive) or red (negative), and hydrophobicity ranges from high (red) to low (white).

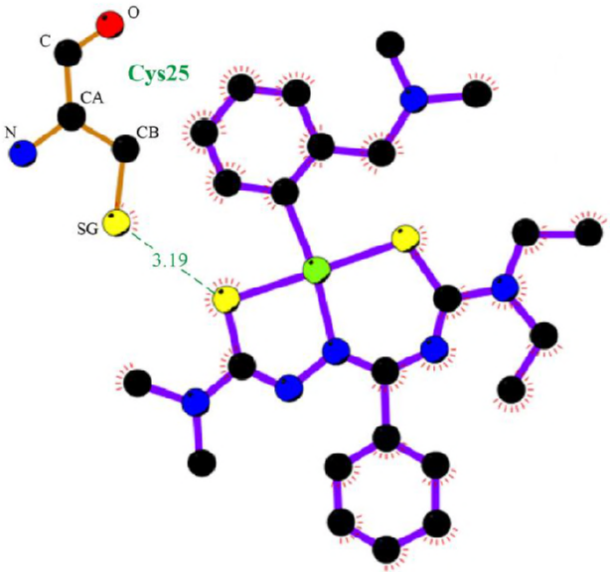

FIG 8. The cruzain active site cysteine Cys25 is predicted to be ~3.0 Å away from the S2 and Au atoms of 4-Cl.

Supplementary Information

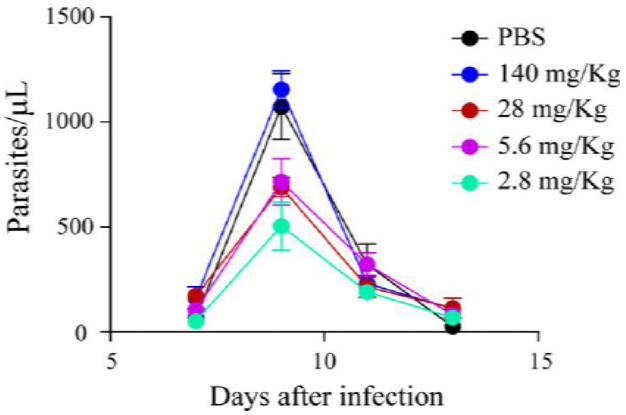

Fig S1. Parasitaemia of mice treated with different concentrations of 4-Cl. The mice (n=5) were treated for 10 consecutive days, starting at 5 days after infection. The choice of concentrations was based on the conversion in molarity of the standard dose of Bz (100 mg/kg). Thus, 140.0 mg refers to a dose five times, 28.0 mg ten times, 5.60 fifty times, and 2.80 a hundred times lower than Bz. The parasitaemia was monitored on days 7, 9, 11 and 13 after infection.

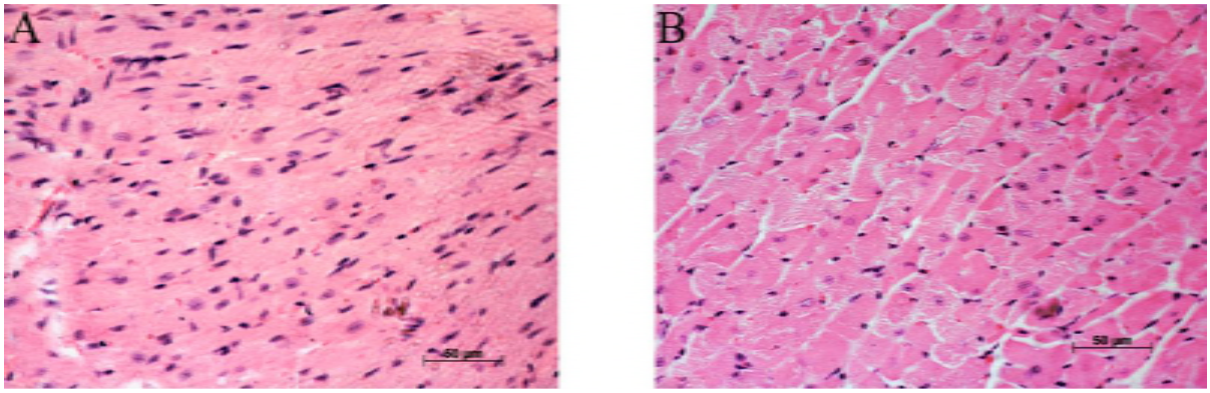

Fig S2. Heart histological sections of treated and surviving mice 150 days after infection. (A) Bz(+) treated-mice; (B) 4-Cl-treated mice.

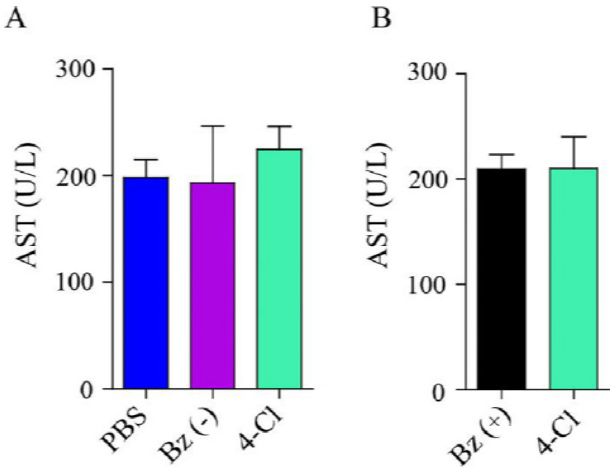

Fig S3. Liver lesions of *T. cruzi*-infected mice after treatment with 4-Cl. (A) Quantification of Aspartate aminotransferase (AST) levels 15 d.p.i. (acute phase, n = 5). (B) Quantification of Aspartate aminotransferase (AST) levels 150 d.p.i. (chronic phase, n = 7).

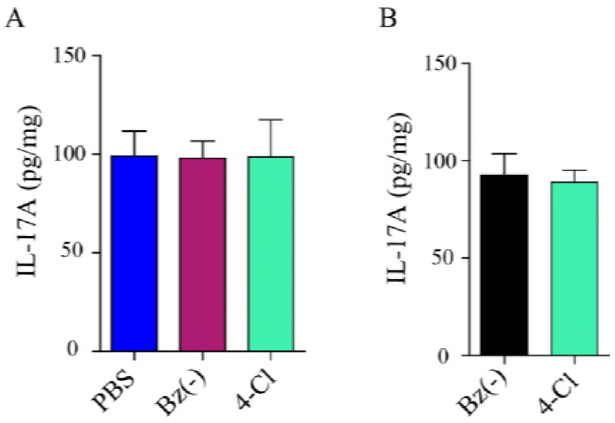

Fig S4. Treatment with 4-Cl did not increase the systemic production of IL-17 in animals infected with *T. cruzi*. IL-17 was measured by ELISA in the serum of Balb/C mice infected and treated with 2.8 mg of Bz and/or 4-Cl. (A) Acute phase - 15 d.p.i. (n = 5) and (B) chronic phase – 150 d.p.i. (n = 7).

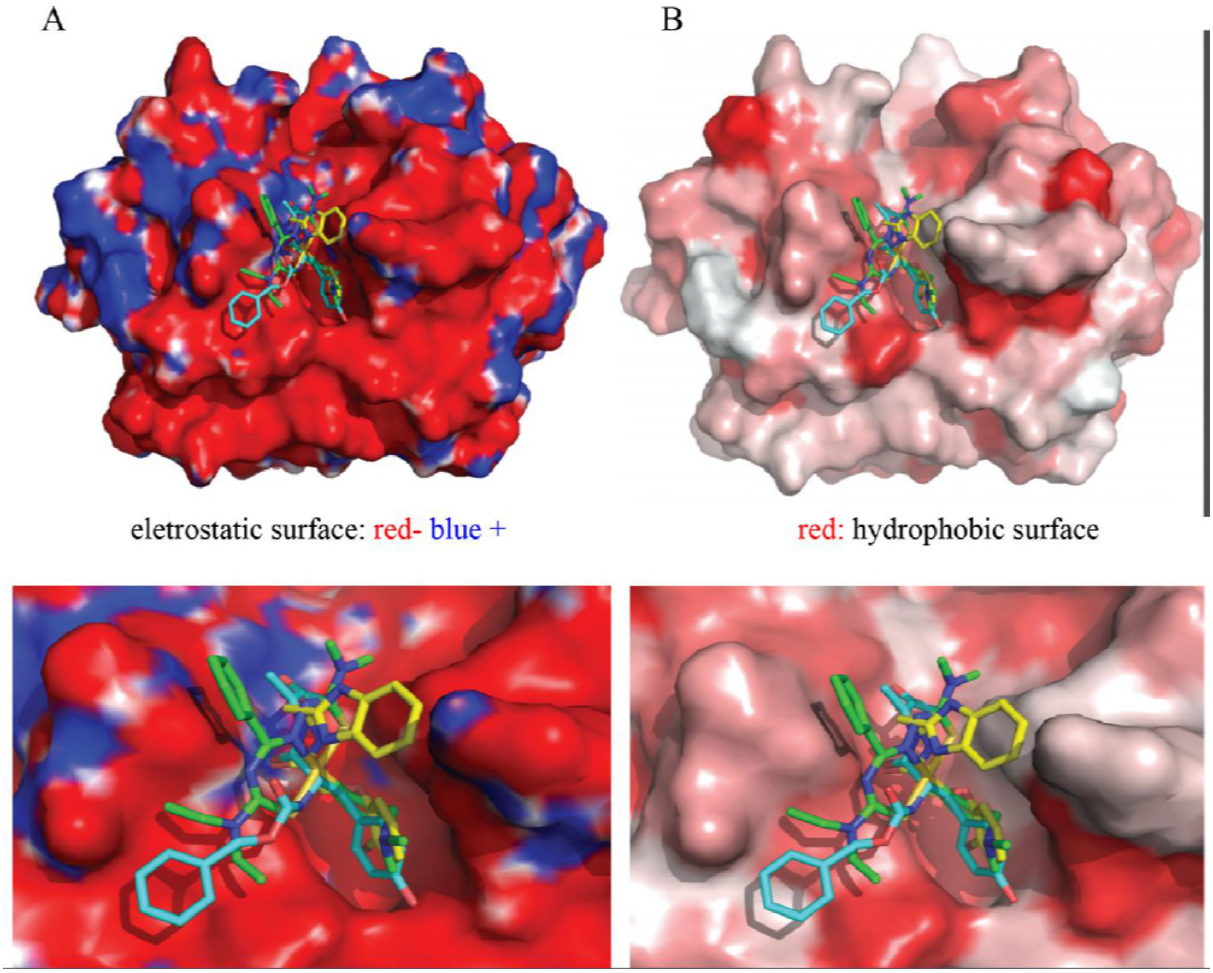

883 **Fig S5.** A) Electrostatic and B) hydrophobic surfaces of the cruzain protease with the
884 following compounds: 4-Cl from this study (green), benzoyl-tyrosine-alanine-
885 fluoromethylketone from the X-ray crystallographic data of cruzain protein used in this
886 study (PDB code 1AIM (31), cyan), benzimidazolethyl-bromophenoxy-acetamide from
887 the X-ray data of cruzain protein used in a high-throughput screen of cruzain inhibitors
888 (PDB code 3KKU (30), yellow).

889

890

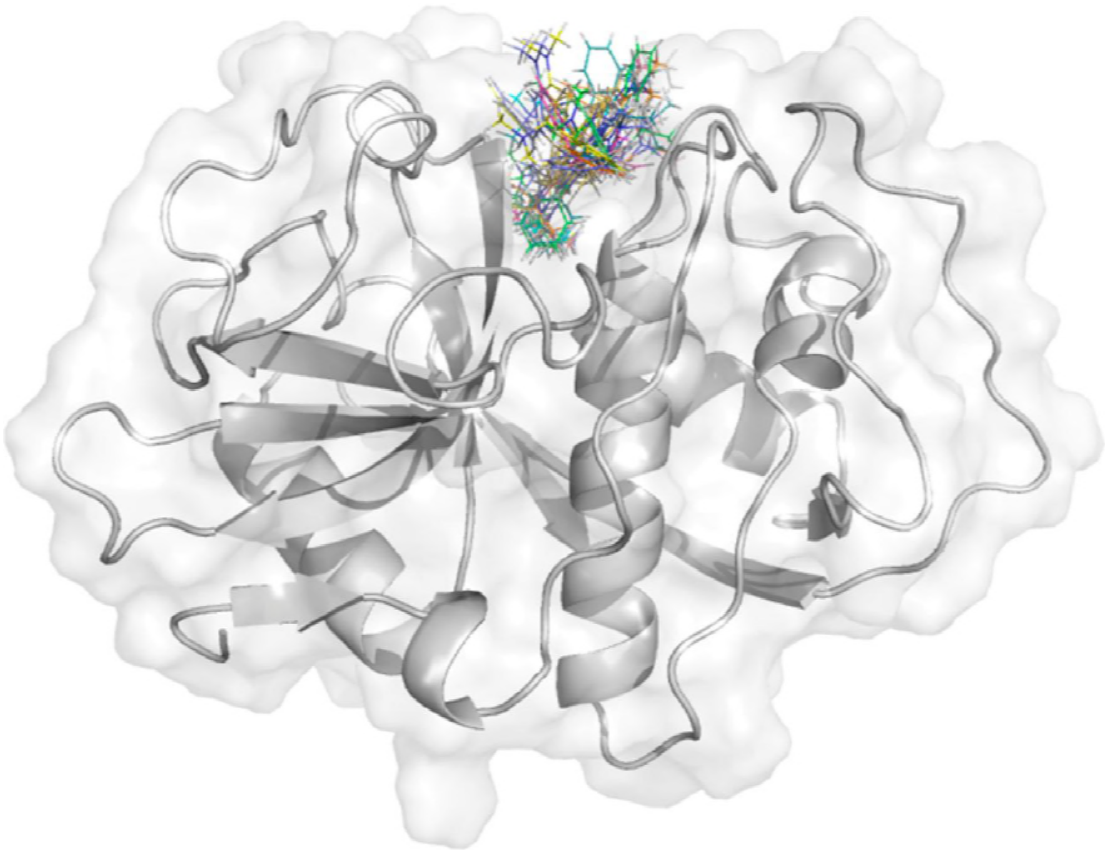

891

892 **Fig S6.** Top 10 best docking solutions of the complex formed by cruzain with
893 [Au(Hdamp)(L)]Cl. All solutions were docked in the primary pocket, the active binding
894 site (29, 30). Compound conformations are shown in lines, and the enzyme is shown in
895 cartoon and surface representations.

896

Docking protocol

Molecular docking simulations of the 4-Cl ligand were carried out to explore the binding modes in the cysteine protease cruzain. The X-ray crystallographic data of the cruzain protease were extracted from the Protein Data Bank (57) (PDB, code 1AIM (31). The compound structure was obtained by single-crystal X-ray studies and prepared with GaussianView 6 software (Gaussian, Inc.) and Marvin Sketch suite version 17.1.27, ChemAxon (http://www.chemaxon.com). The docking simulations were performed with the GOLD suite version 5.5 in the enzyme active site. Pre- and post-docking visualisation and interactive docking setup were conduct with Hermes software from the GOLD suite. All water molecules and heteroatoms were removed from the protease. Only residues within 6.0 Å surrounding the native inhibitor were used as the ligand cavity site. The Genetic Algorithm (GA) method was used to run the calculations (30). Full flexibility was allowed to the ligand. GA runs conducted herein with a maximum of 100,000 GA operations were performed on a population size of 100 individuals. Diverse solutions were generated, ring corners were allowed to flip, conformations were explored, and no constraint was applied to the protein or to the ligands. Redocking simulations of the native inhibitor from the PDB code 1AIM were executed in the enzyme active site with all the available GOLD score functions, and the best score (lowest rmsd to the X-ray conformation) was found with the GoldScore fitness function rescored by ChemScore (49). Thus, GoldScore rescored by the ChemScore fitness function was chosen to predict the binding mode of the compound in the study with the cruzain crystallographic structure. The GoldScore ranking was evaluated and the best pose, the highest-ranking structure for the compound, was chosen for the interaction analysis. Figures of the cruzain protease/inhibitor complexes were prepared with PyMOL (Molecular Graphics System, version 1.8 Schrödinger, LLC).

922

923 **FIG 1.**

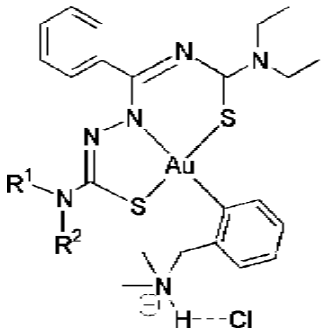

1-Cl: R^1 = Me, R^2 = Ph
2-Cl: R^1R^2 = $(CH_2)_5$
3-Cl: R^1R^2 = $(CH_2)_6$
4-Cl: R^1 = R^2 = Me
5-Cl: R^1 = R^2 = *n*-propyl

924

925

926 **FIG 2.**

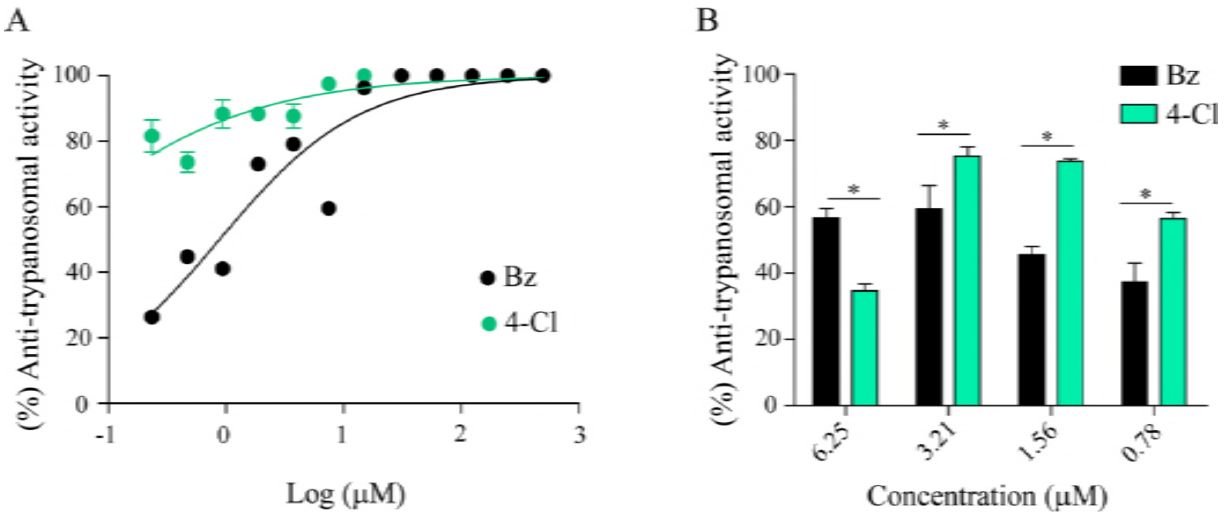

927

928

929 **FIG 3.**

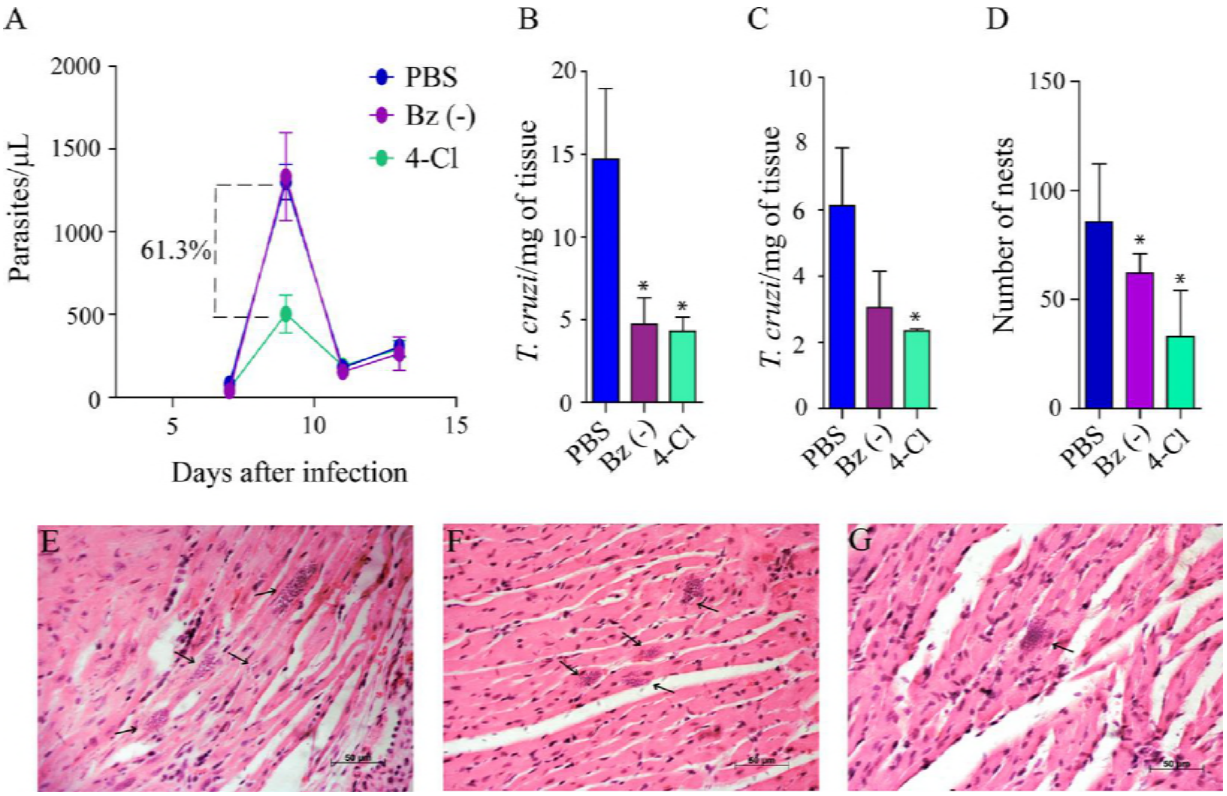

930

931

932 **FIG 4.**

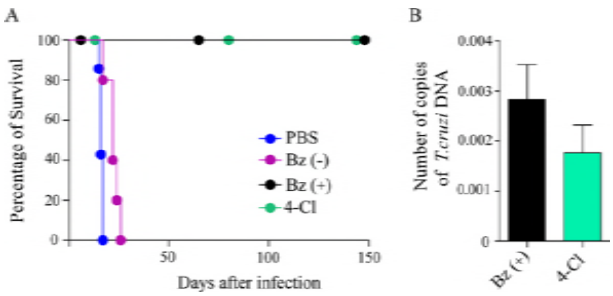

933

934 **FIG 5.**

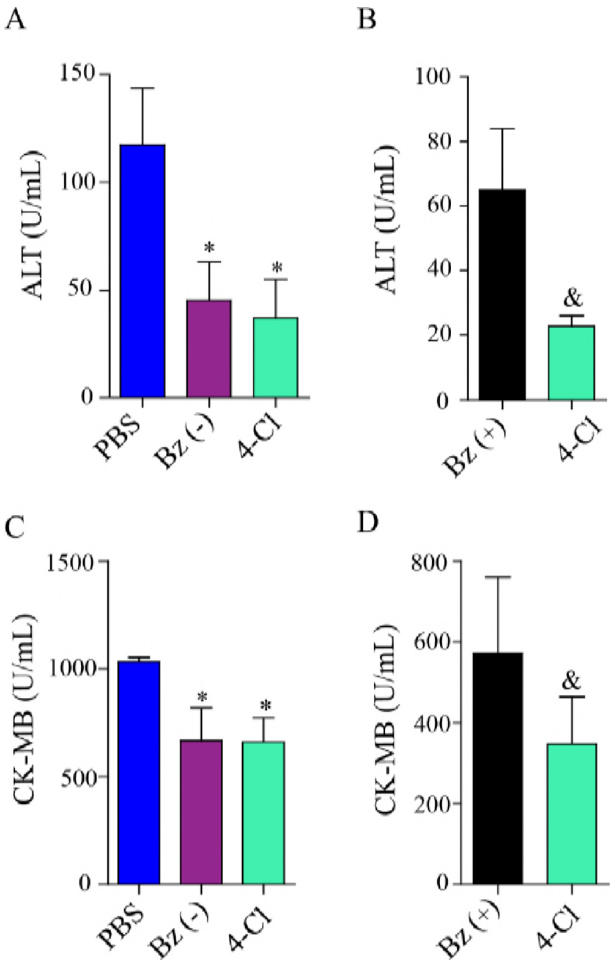

935

936

937 **FIG 6.**

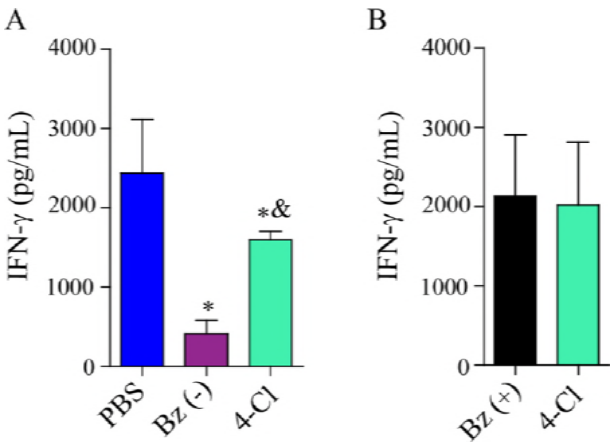

938

939

940 **FIG 7.**

941

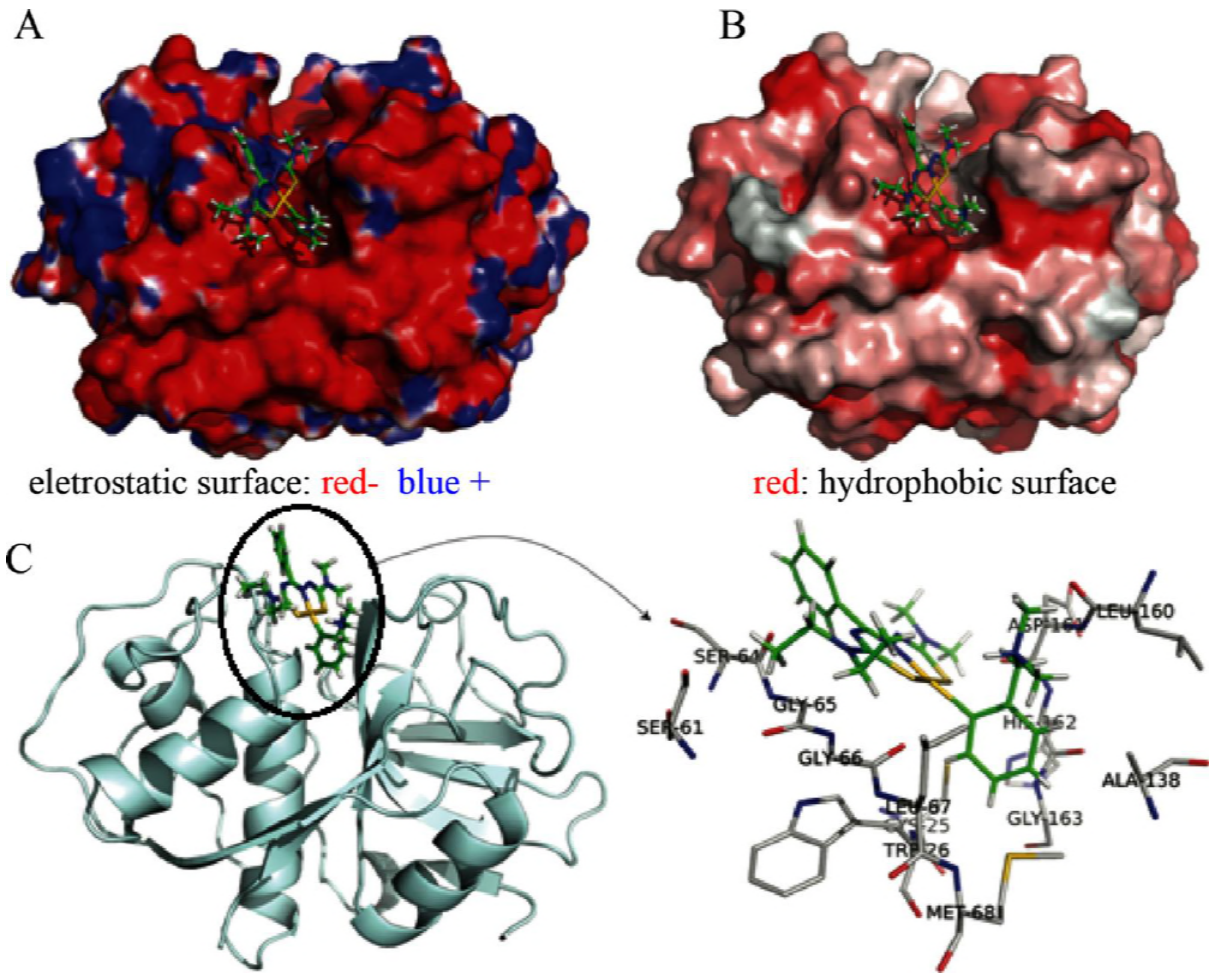

942

943 **FIG 8.**

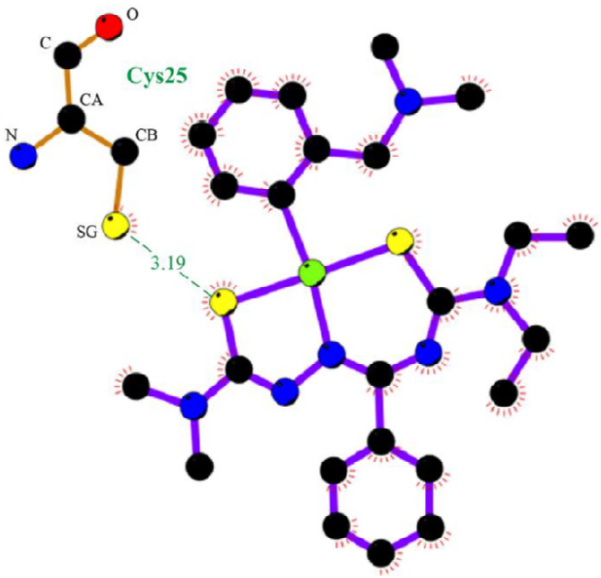

944

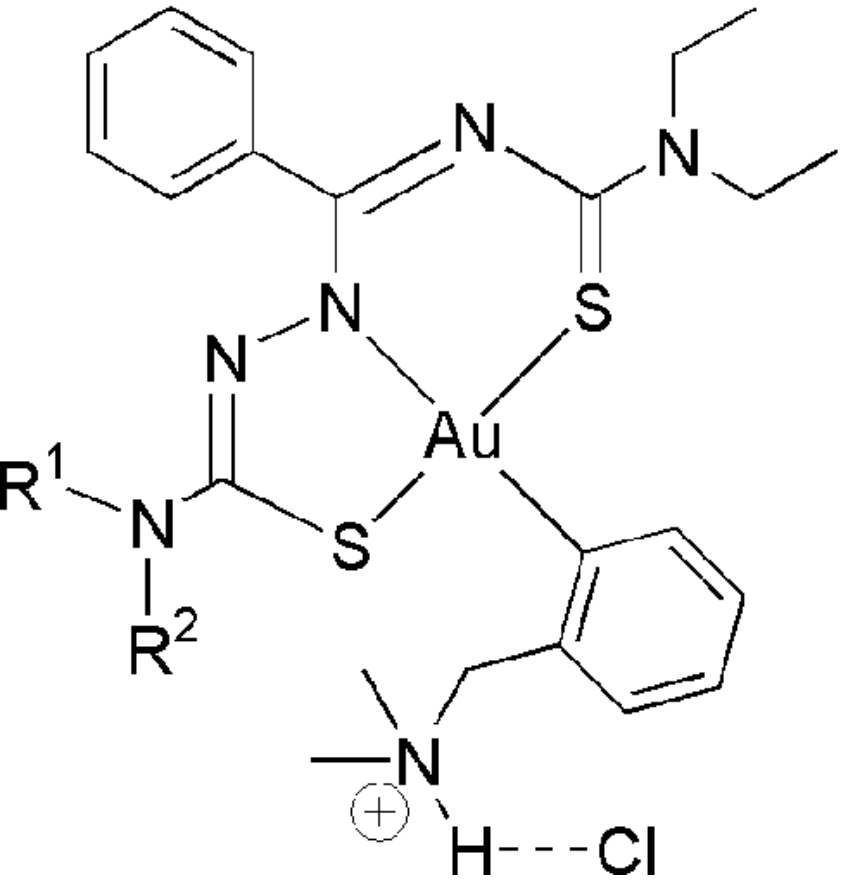

1-Cl: R^1 = Me, R^2 = Ph

2-Cl: R^1R^2 = $(CH_2)_5$

3-Cl: R^1R^2 = $(CH_2)_6$

4-Cl: R^1 = R^2 = Me

5-Cl: R^1 = R^2 = *n*-propyl

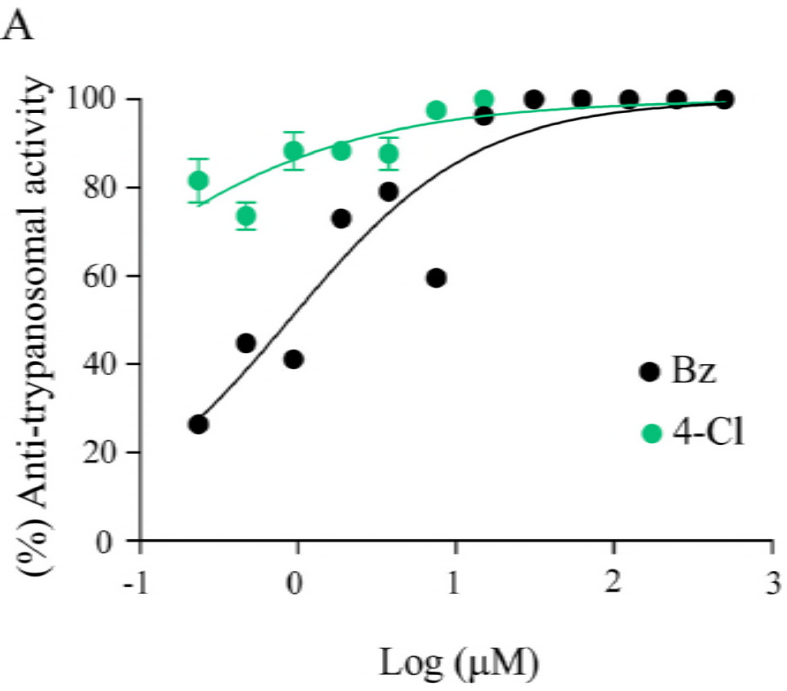
A
(%) Anti-trypanosomal activity
100
80
60
40
20
0
-1
0
1
2
3
Log (µM)
Bz
4-Cl

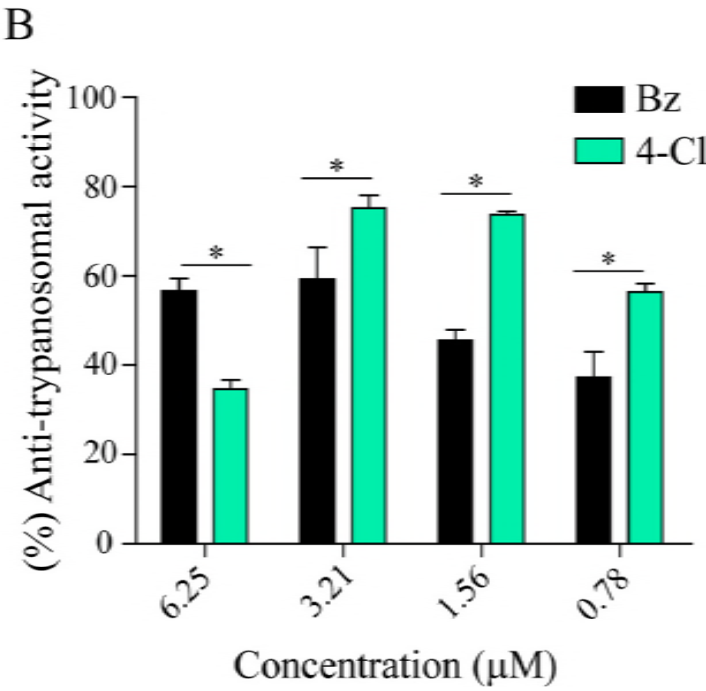
B
(%) Anti-trypanosomal activity
100
80
60
40
20
0
*
*
*
*
6.25
3.21
1.56
0.78
Concentration (µM)
Bz
4-Cl

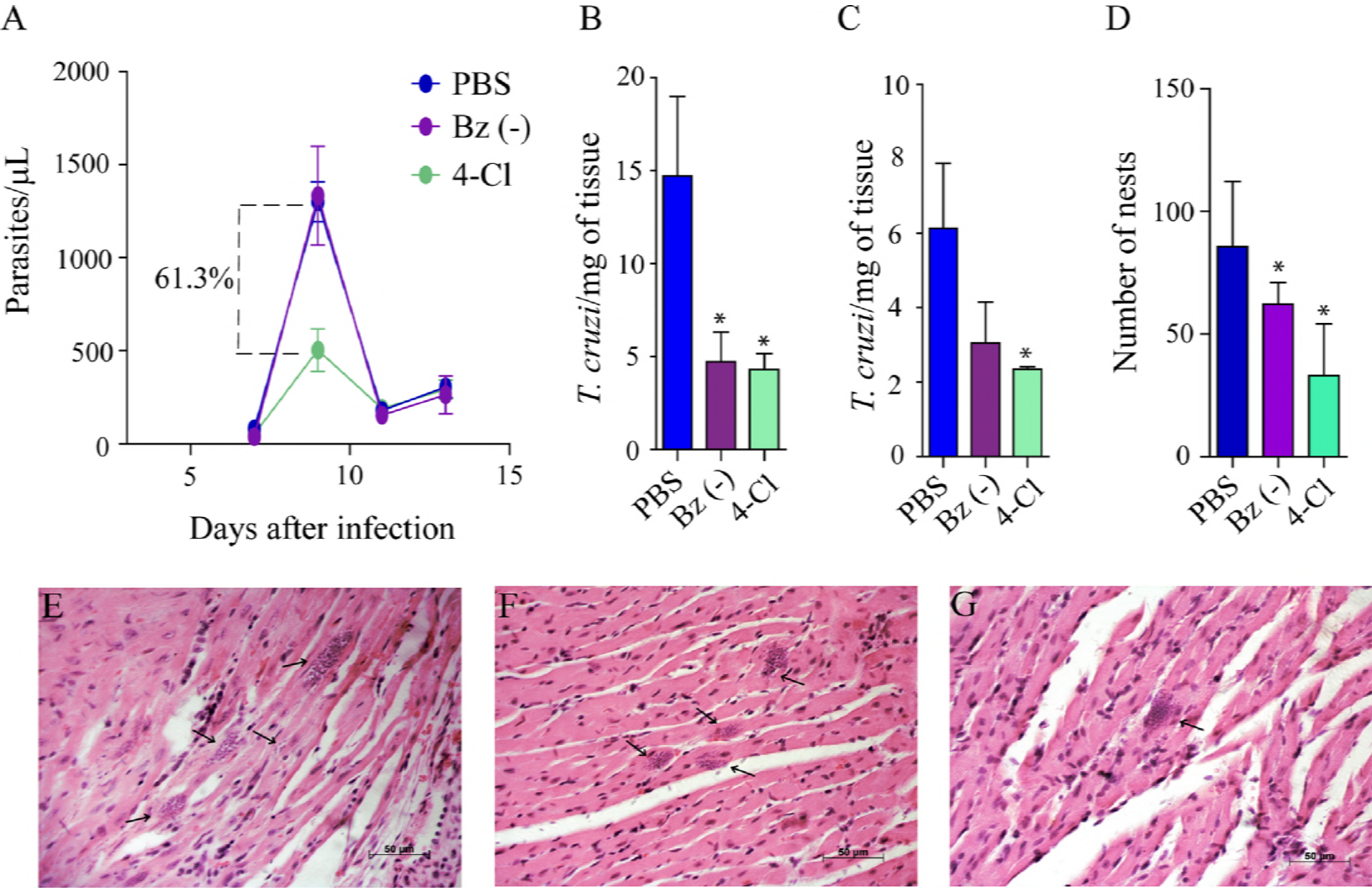
A
B
C
D
2000
1500
1000
500
0
Parasites/µL
PBS
Bz (-)
4-Cl
61.3%
5
10
15
Days after infection
20
15
10
5
0
T. cruzi/mg of tissue
*
*
PBS
Bz (-)
4-Cl
10
8
6
4
2
0
T. cruzi/mg of tissue
*
*
PBS
Bz (-)
4-Cl
150
100
50
0
Number of nests
*
*
PBS
Bz (-)
4-Cl

E
50 µm

F
50 µm

G
50 µm

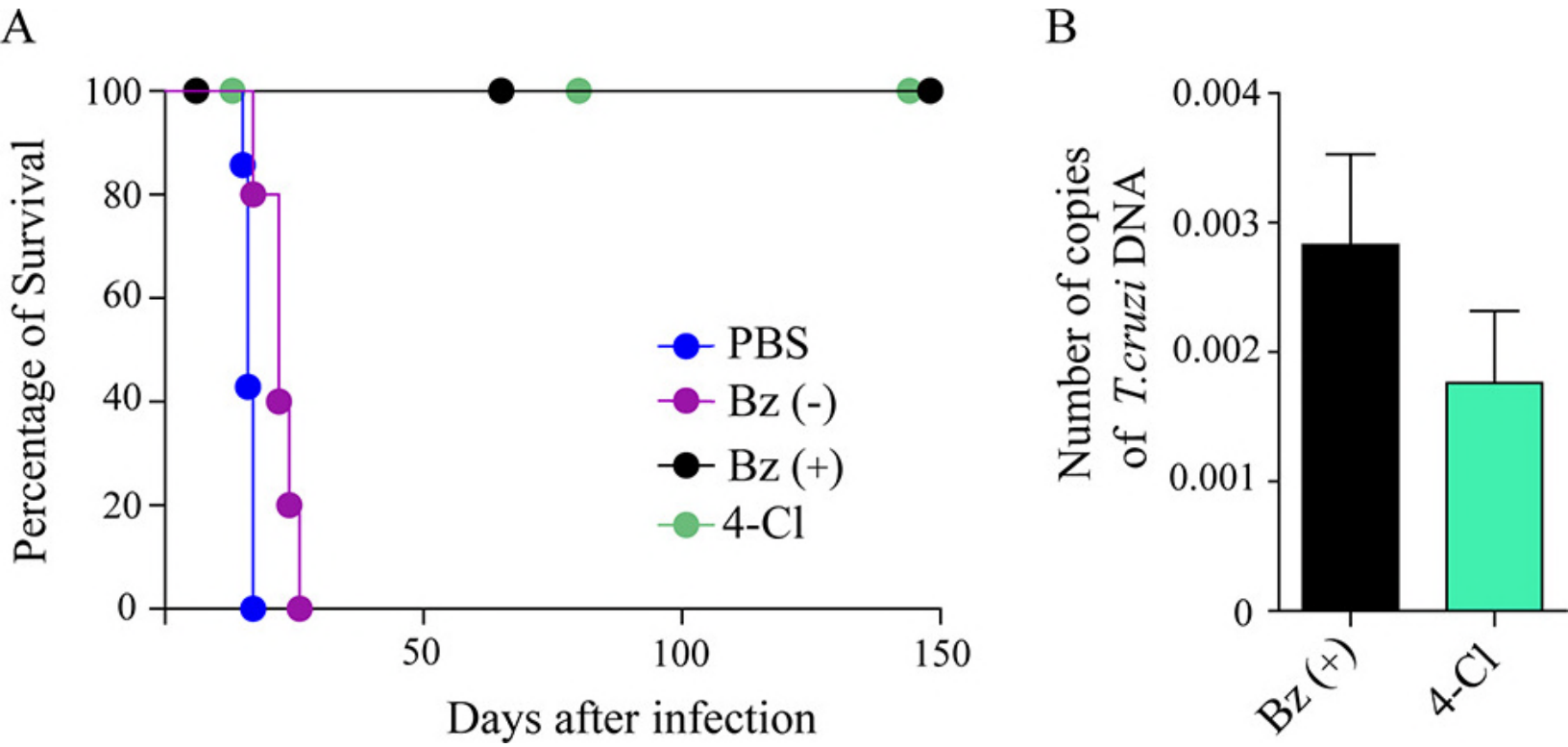
A
Percentage of Survival
100
80
60
40
20
0
50
100
150
Days after infection
PBS
Bz (-)
Bz (+)
4-Cl
B
Number of copies of T.cruzi DNA
0.004
0.003
0.002
0.001
0
Bz (+)
4-Cl

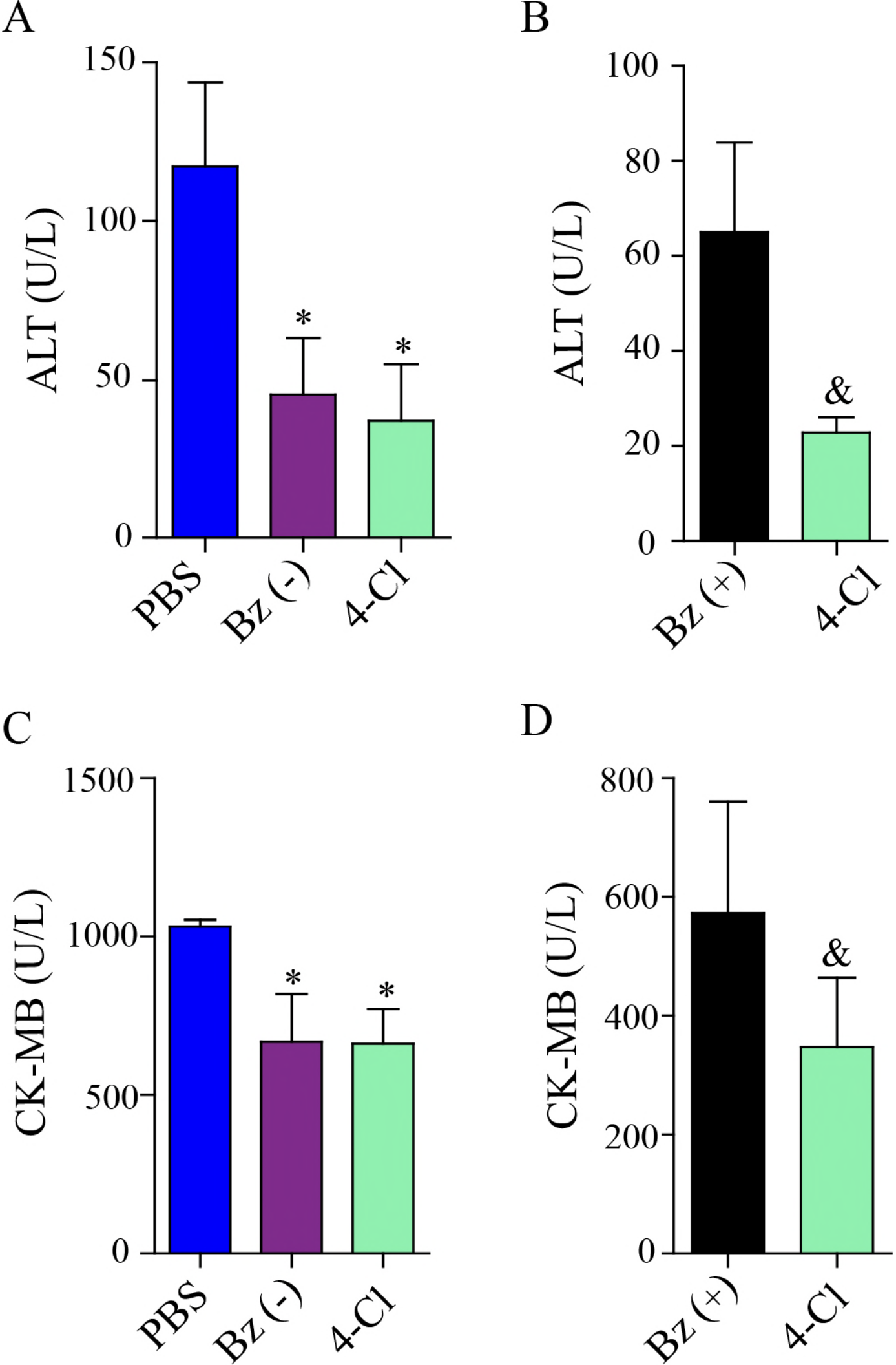
A
150
100
50
0
ALT (U/L)
*
*
PBS
Bz (-)
4-Cl
B
100
80
60
40
20
0
ALT (U/L)
&
Bz (+)
4-Cl
C
1500
1000
500
0
CK-MB (U/L)
*
*
PBS
Bz (-)
4-Cl
D
800
600
400
200
0
CK-MB (U/L)
&
Bz (+)
4-Cl

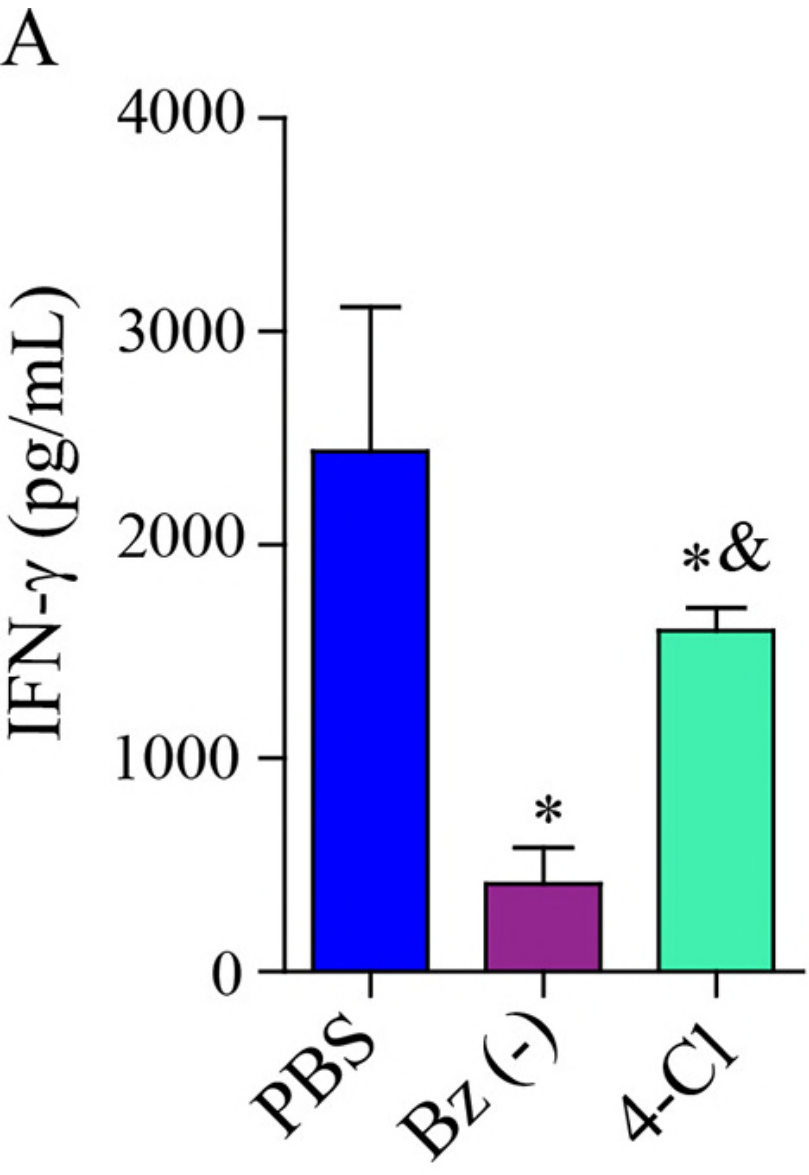
A
4000
3000
2000
1000
0
IFN-γ (pg/mL)
*
*&
PBS
Bz (-)
4-Cl

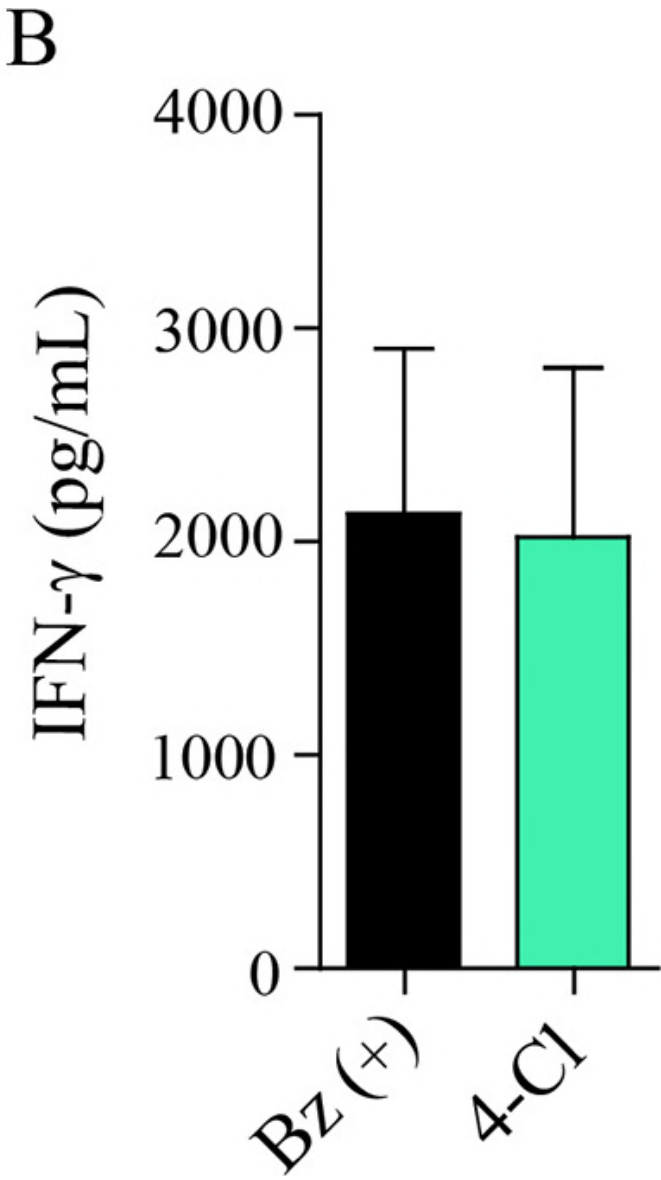
B
4000
3000
2000
1000
0
IFN-γ (pg/mL)
Bz (+)
4-Cl

A

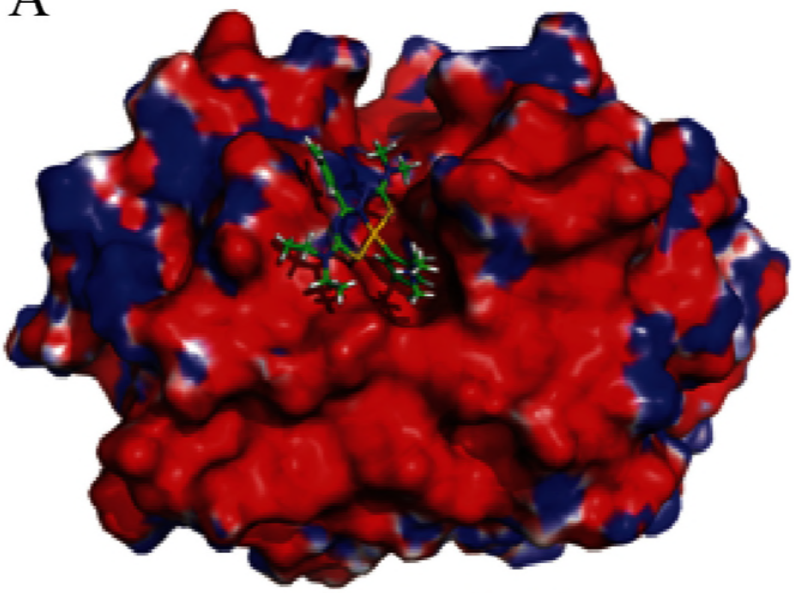

B

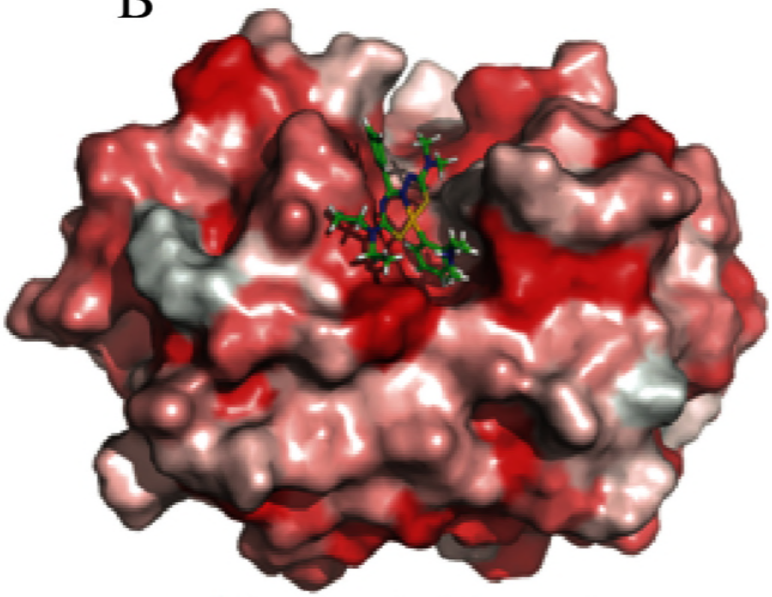

eletrostatic surface: red- blue +

red: hydrophobic surface

C

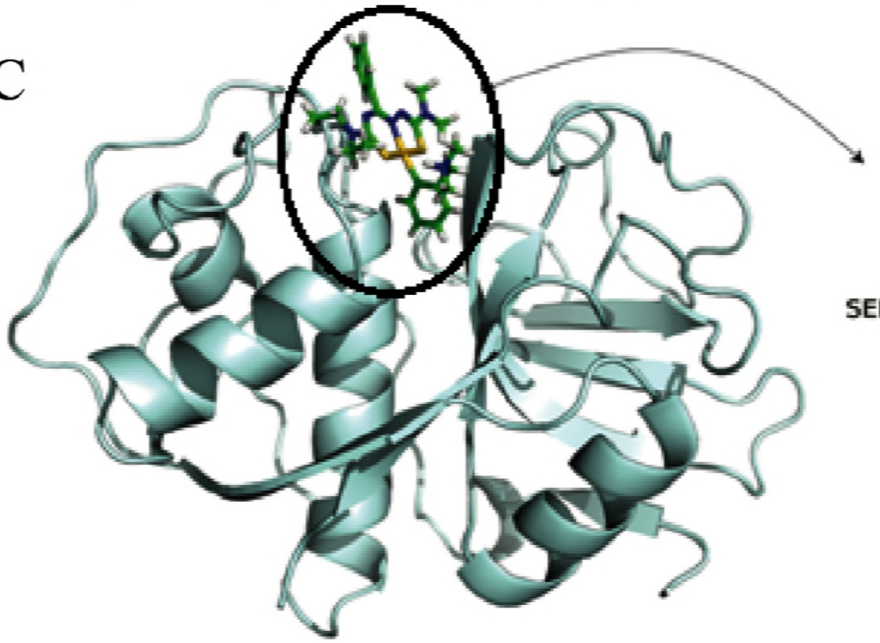

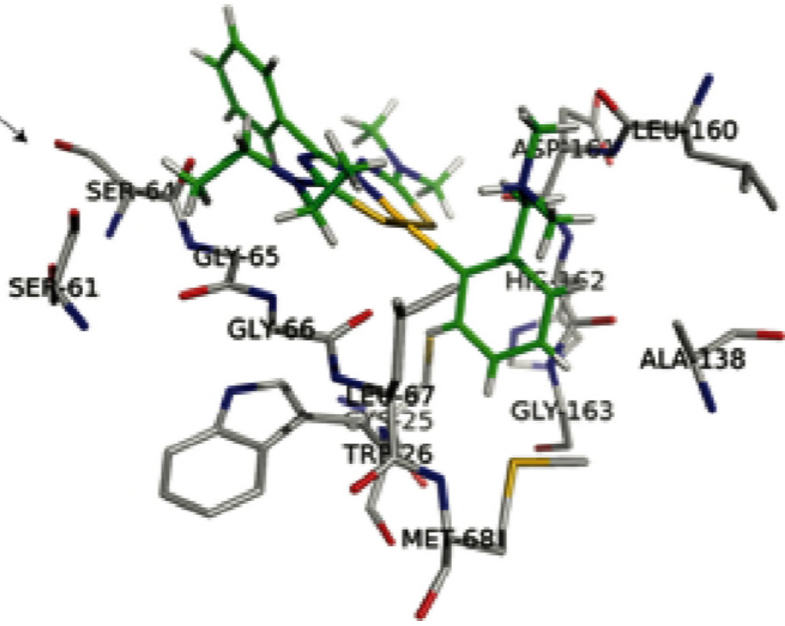

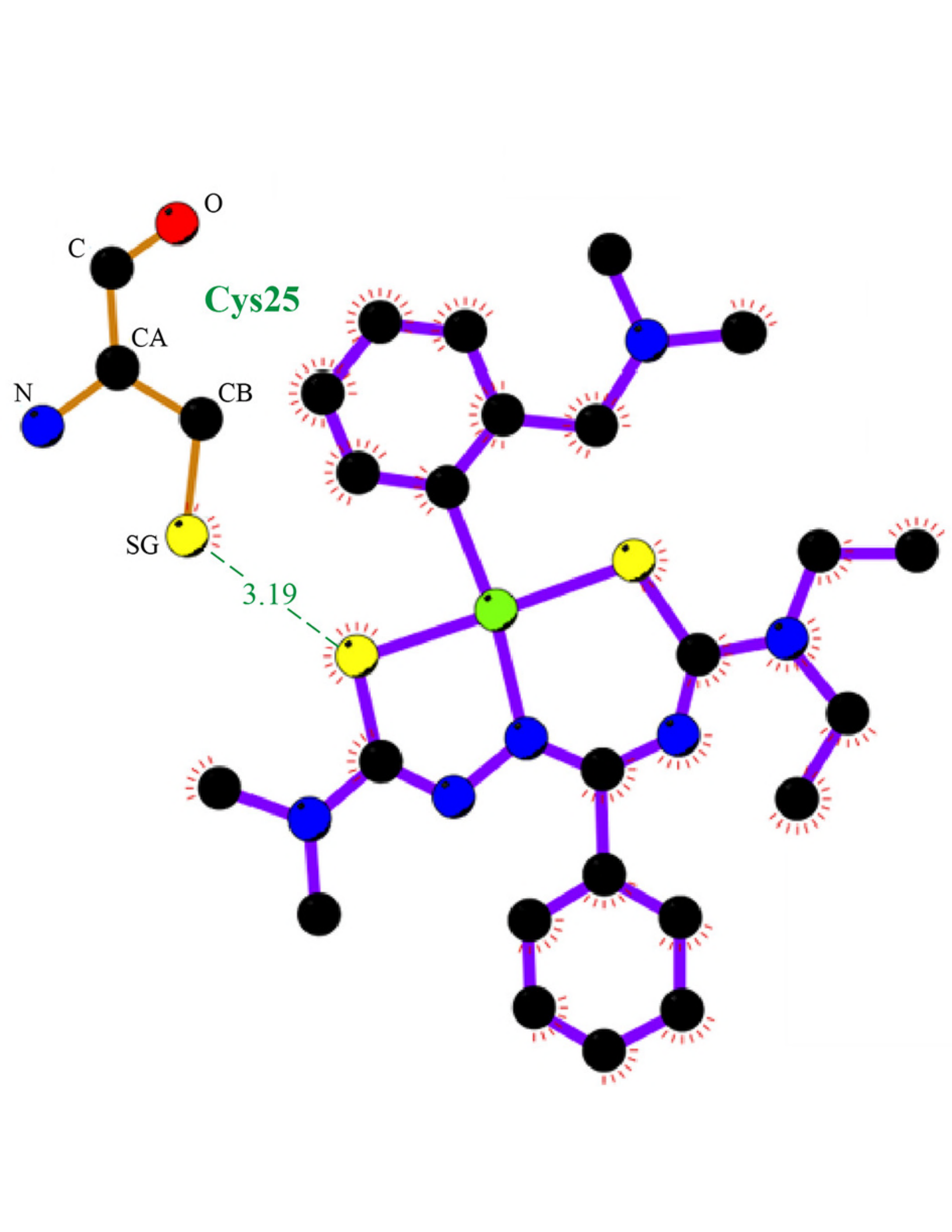
O
C
Cys25
CA
N
CB
SG
3.19